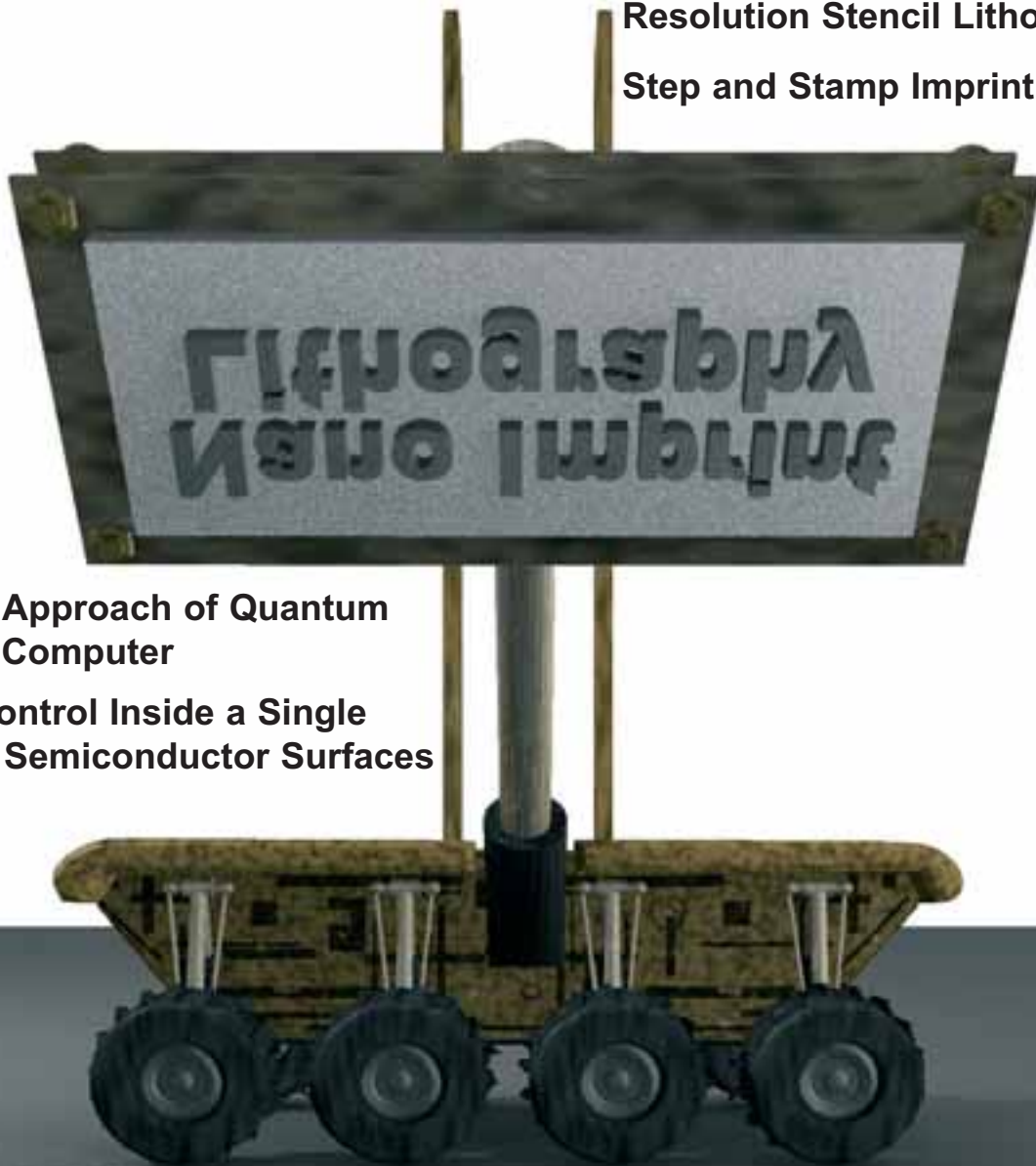




Quick & Clean: Advances in High Resolution Stencil Lithography

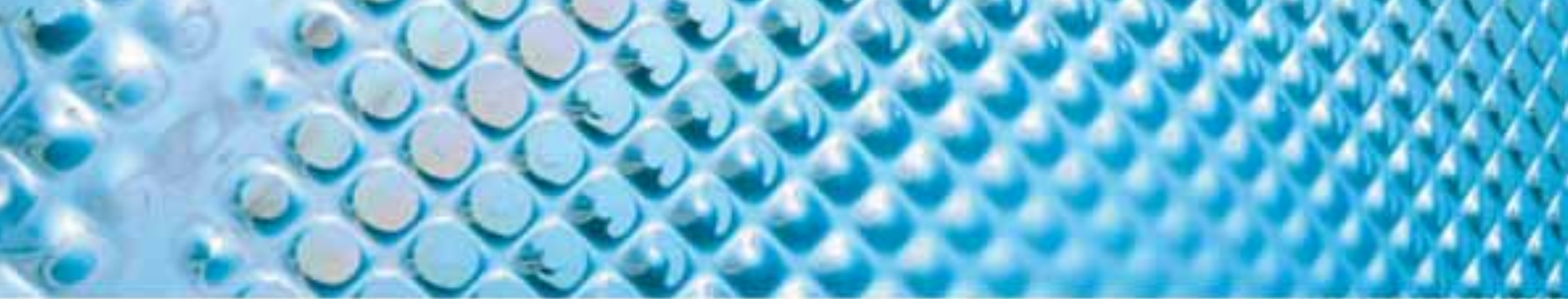
Step and Stamp Imprint Lithography



Geometrical Approach of Quantum Hamiltonian Computer

Electronic Control Inside a Single Molecule on Semiconductor Surfaces





CIC

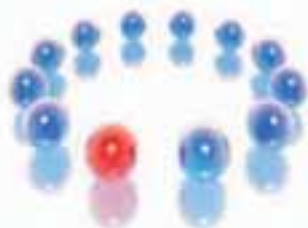
nanogUNE

nanoscience COOPERATIVE RESEARCH CENTER

The Nanoscience Cooperative Research Center **CIC nanoGUNE Consolider** invites applications and nominations for three positions as

Group Leaders

CIC nanoGUNE Consolider, located in San Sebastian, Basque Country (Spain), is a R&D center created recently with the mission of addressing basic and applied strategic world-class research in nanoscience and nanotechnology, fostering high-standard training and education of researchers in the field, and supporting the growth of a nanotechnology-based industry.



The Group Leaders of nanoGUNE will be responsible for the design, management and operation of their respective Research Area and laboratories. At the present time, nanoGUNE is welcoming applicants in the following disciplines:

- Nanofabrication and nanostructure assembly (#001)
- Synthesis of nanomaterials and nanostructures (#002)
- Biological nanostructures and nanobiotechnology (#003)

Candidates should have an outstanding track record of research, with an orientation to nanoscience and nanotechnology, a proven ability to obtain competitive research funding, and a proven record of technological transfer initiatives. Proficiency in spoken and written English is compulsory; knowledge of Spanish is not a requirement. An attractive remuneration will be offered.

Applicants should forward their CV, a summary of research interests and a list of at least three references to director@nanogune.eu

E *nano* newsletter

Editorial Information	3
Pico-Inside Integrated Project	
Geometrical Approach of Quantum Hamiltonian Computer	5
<i>N. Renaud, P. Solinas, R. Mosseri and C. Joachim</i>	
Electronic Control Inside a Single Molecule on Semiconductor Surfaces	11
<i>A. Bellec, F. Chiaravalloti, G. Dujardin and D. Riechel</i>	
NANO Vacancies	18
NANO Conferences	20
NANO News	21
NaPa Integrated Project	
Quick & Clean: Advances in High Resolution Stencil Lithography	22
<i>J. Brugger, V. Savu, K. Sidler, M. Van den Boogaart, O. Vazquez and G. Villanueva</i>	
Step and Stamp Imprint Lithography	28
<i>T. Haatainen, P. Majander, G. Lecarpentier and J. Ahopelto</i>	
Research Review	
Diving into the Realm of Nanosciences: Understanding of Electronic and Transport Properties of Nanotubes	34
<i>A. Correia</i>	

Dear Readers:

This E-Nano Newsletter issue is mainly dedicated to provide insights in molecular electronics (computing inside a single molecule) and alternative nanofabrication techniques pushed into the sub-100nm scale ("stencil" and "step and stamp imprint" lithography) within 2 EU funded Integrated Projects - Pico-Inside and NaPa respectively.

In addition, a short introduction to the recent review article by J.C. Charlier et al. on Carbon Nanotubes and Technology is presented.

We would like to thank all the authors who contributed to this issue as well as the European Union (FET/NanoICT) and the Pico-Inside and NaPa projects for their close collaboration.

Dr. Antonio Correia

E *nano* newsletter Editor

Phantoms Foundation

Deadline for manuscript submission:

Issue n°10: October 01, 2007

Issue n°11: December 01, 2007

Depósito Legal: M-43078-2005

Editorial Board: Adriana Gil (Nanotec SL, Spain), Christian Joachim (CEMES-CNRS, France), Ron Reifenger (Purdue University, USA), Stephan Roche (CEA-DRFMC, France), Juan Jose Saenz (UAM, Spain), Pedro A. Serena (ICMM-CSIC, Spain), Didier Tonneau (CRMC2-CNRS, France), Rainer Waser (Research Center Julich, Germany)

For any question please contact the editor at:

antonio@phantomsnet.net

EDITORIAL INFORMATION

E *nano* newsletter n°8 June 2007

Published by **Phantoms Foundation** (Spain)

Editor: Dr. Antonio Correia (Phantoms Foundation)

antonio@phantomsnet.net

Assistant Editor: Jose Luis Roldan (Phantoms Foundation)

jlroldan@phantomsnet.net

1500 copies of this issue have been printed

MC2 ACCESS

**To research groups in
EU, associate and candidate countries:**

**We offer free access to advanced
processing for microwave electronics,
photonics and nanotechnology.**

Through an EU-financed programme we offer free access to advanced micro- and nanotechnology device processing environments for microwave and photonic devices, MEMS structures and for nanotechnology at the Department of Microtechnology and Nanoscience (MC2), Chalmers University of Technology, in Göteborg, Sweden. This offer is open for visiting researchers as well as remote users, both from universities and SMEs (small and medium size enterprises).

The facility provides means to develop process steps, process sequences, and components in small/medium quantities. In 1240 m² of clean-room area, more than 170 tools are available, including two e-beam lithography systems, silicon processing on up to 150 mm wafers, III-V and wide bandgap processing, molecular beam epitaxy, CVD and dry etching systems.

Only research groups that are entitled to disseminate the knowledge they have generated under the project are eligible to benefit from access to the infrastructure under the contract. **NOTE!** The sole exception to this rule are user groups from an SME that wish to use the infrastructure for the first time.

Contract No: 026029

Contract Period: 2006-2009



Project Manager:

Associate Professor

Ulf Södervall

access@mc2.chalmers.se

MC2
Microtechnology and Nanoscience



Geometrical Approach of Quantum Hamiltonian Computer

N. Renaud (1), P. Solinas (2), R. Mosseri (2) and C. Joachim (1)

(1) CEMES/CNRS, 29 rue Jeanne Marvig, 31055 Toulouse (France)
 (2) LPTMC/CNRS and UPMC, 4 Place Jussieu, 75252 Paris (France)

1. Introduction

Recent progresses in atomic-scale technologies are opening the possibility to control the intrinsic time evolution of a unique quantum system like a single molecule. This evolution, described by the time dependant Schrödinger equation, can be used to realize a quantum logic gate. In one design studied by Pico-Inside, the energy necessary for the quantum system to compute is brought by the preparation of a non-stationary state, the data are encoded directly in the Hamiltonian and the results of the calculation are measured on the occupation probability of the system on the target states beforehand defined [1] [2].

In this Quantum Hamiltonian Computer (QHC) approach, it can be easily shown that, in order to compute, the system requires at least three quantum states. A complete representation of the evolution of this system on its quantum state space is required to appreciate how the quantum trajectory is controlled by the input. Without losing

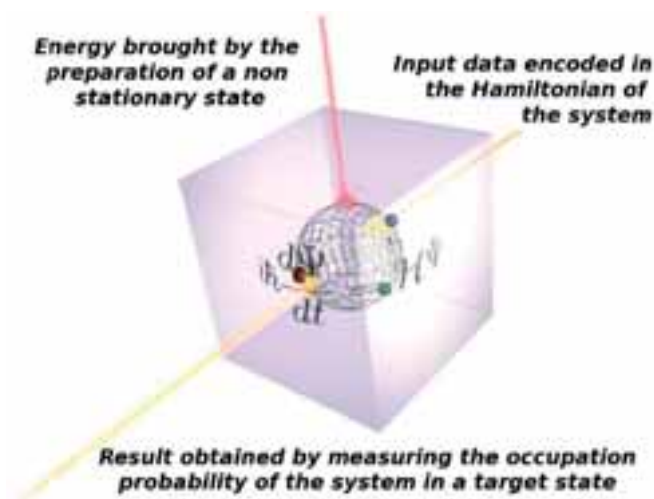


Figure 1: General scheme for a quantum Hamiltonian computer

information, the Bloch representation can only map the evolution of two states systems. In Pico-Inside we are exploring an other approach, adapted from a representation originally proposed by E. Majorana in 1932 [4] in the context of high spin systems, and which allows to completely describe the evolution of a N states system.

2. Design of a Quantum Hamiltonian Logic Gate

Like any quantum machine, a QHC needs energy to work [3]. An elegant solution to supply this energy is to initially prepare the system, described by a Hamiltonian \mathcal{H} in a non stationary state $|\Psi_0\rangle$ increasing its energy with respect to its ground state energy. This state can be written on the eigenbasis of the system, $\{...|\Phi_n\rangle...\}$, as:

$$|\psi_0\rangle = \sum_n a_n(0)|\phi_n\rangle \quad (1)$$

The system will then evolve spontaneously, following the time dependant Schrödinger equation:

$$i\hbar \frac{d|\psi(t)\rangle}{dt} = \mathcal{H}|\psi(t)\rangle \quad (2)$$

leading to the standard expression for $|\Psi(t)\rangle$:

$$|\psi(t)\rangle = e^{-i\mathcal{H}t/\hbar}|\psi_0\rangle = \mathcal{U}(t)|\psi_0\rangle \quad (3)$$

where $\mathcal{U}(t)$ is the evolution operator which drives the evolution through the Hilbert space. For this evolution to allow for a computation process, the input data have to be encoded somewhere in the system. This can be done either in the Hamiltonian \mathcal{H} or in the initial state $|\Psi_0\rangle$. In the QHC approach, the first strategy is followed: the initial state is fixed (among the local basis states) whereas the Hamiltonian $\mathcal{H}(\theta_1, \theta_2, \dots, \theta_n)$ depends of the input data θ_i . Starting from this constant initial state, the system therefore experiences different time evolutions (distinct paths through the Hilbert space) depending on the Hamiltonian. This is in sharp contrast with the well known quantum computer qubit approach where unitary transforms associated with the different logical gates are driven by constant Hamiltonians, while the input data are coded in the initial state $|\Psi_0(\theta_1, \theta_2, \dots, \theta_n)\rangle$ (in addition, handling linear combination of basis states is central in that approach).

The simplest way in which the result of the computation could be read from the system time evolution is to measure the population, $P(t)$, of a beforehand defined target state, at a specific measurement time (called here t_m). Besides, periodic evolutions should allow to perform the measurement not only at t_m but at each odd multiple of t_m

$$P(t_m) = |\langle \psi_{\text{target}} | \mathcal{U}(\theta_1, \theta_2 \dots \theta_n)((2k+1)t_m) | \psi_0 \rangle|^2 \quad (4)$$

One expects for instance that the population of the target state reaches exactly one, whenever the (logical) result of the computation is expected to be one, and be zero otherwise. Note once again that the above expression supposes that one has been able to define a system which behaves periodically with a quantum state oscillation between the initial and the target state.

The general scheme of a quantum Hamiltonian computer is illustrated in Fig. 1.

3. Realisation of a quantum Hamiltonian XOR gate

To give a clear example of a QHC, we present here a simple analytical model of an XOR gate embodied in a four level system. The truth table of a such gate is recalled on **Fig. 2**. We have studied the four level quantum system shown in **Fig. 3** represented by the Hamiltonian 5, where μ and e are fixed parameters, and α and β are the two parameters which will be used to encode the input data of the computation.

input 1	input 2	output
0	0	0
0	1	1
1	0	1
1	1	0

Figure 2: Truth table of a XOR gate

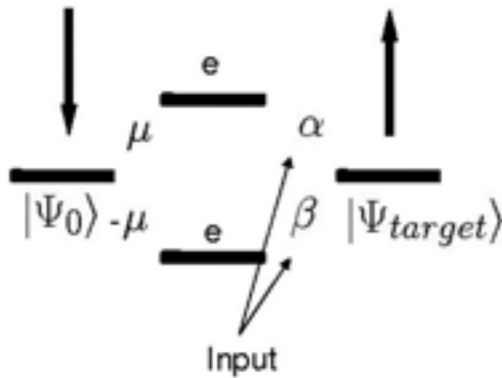


Figure 3: Four level system chosen to perform a XOR gate

$$\mathcal{H} = \hbar\omega \begin{pmatrix} 0 & \mu & -\mu & 0 \\ \mu & e & 0 & \alpha \\ -\mu & 0 & e & \beta \\ 0 & \alpha & \beta & 0 \end{pmatrix} \quad (5)$$

The initial state is the first state of the basis and the target state is the last one. The input data can be either encoded in the phase of the two parameters α and β or in the strength of those couplings. In the following we present Hamiltonian \mathcal{H} generating periodic evolution leading to $P(t_m) = 1$. It can be proved that a periodic evolution is obtained for commensurate eigenvalues of the Hamiltonian.

3.1 Encoding in the phase of the couplings

If one only allows for phase control in the Hamiltonian entries, the inputs parameters can be written as: $\alpha = e^{i\phi_1}$ and $\beta = e^{i\phi_2}$. In this case the Hamiltonian is:

$$\mathcal{H} = \hbar\omega \begin{pmatrix} 0 & \mu & -\mu & 0 \\ \mu & e & 0 & e^{i\phi_1} \\ -\mu & 0 & e & e^{i\phi_2} \\ 0 & e^{-i\phi_1} & e^{-i\phi_2} & 0 \end{pmatrix} \quad (6)$$

The eigenvalues of this system are given by:

$$\lambda = \hbar\omega \frac{e}{2} \pm \frac{1}{2} \hbar\omega \sqrt{e^2 + 4\{(1 + \mu^2) \pm \sqrt{1 + \mu^4 - 2\mu^2 \cos(\phi_1 - \phi_2)}\}} \quad (7)$$

To simplify the study of the eigenvalues commensurability, we can impose $e=0$. Note, nevertheless, that this is not a necessary condition and equivalent results could be reached with $e \neq 0$. In the 00 and 11 configurations, so when $\phi_1 = \phi_2 = \phi$, the result of the computation must be equal to zero. In this case the eigenvalues are given by the simple formula: $\lambda = \hbar\omega 2^{1/2} [-\mu, -1, 1, \mu]$. Computing the evolution of the system of the target state we find it is never populated along the evolution. To understand this interference phenomenon we can apply a $\pi/4$ rotation defined by:

$$\mathcal{R}(\theta) = \begin{pmatrix} 1 & 0 & 0 & 0 \\ 0 & \cos(\theta) & \sin(\theta) & 0 \\ 0 & -\sin(\theta) & \cos(\theta) & 0 \\ 0 & 0 & 0 & 1 \end{pmatrix} \quad (8)$$

on the two central state of the Hamiltonian. This rotation do not change the initial and the final state, applying the rotation we find:

$$\begin{aligned} \tilde{\mathcal{H}} &= \mathcal{R}^\dagger\left(\frac{\pi}{4}\right)\mathcal{H}\mathcal{R}\left(\frac{\pi}{4}\right) \\ &= \sqrt{2}\hbar\omega \begin{pmatrix} 0 & \mu & 0 & 0 \\ \mu & 0 & 0 & 0 \\ 0 & 0 & 0 & e^{i\phi} \\ 0 & 0 & e^{-i\phi} & 0 \end{pmatrix} \end{aligned} \quad (9)$$

So as the initial and the target state are still the first and the last on the basis we clearly see here that they are not connected by the Hamiltonian. This explain why the population of the target state remains zero during the evolution. In the two others configurations, i.e when $\phi_1 \neq \phi_2$, the eigenvalues are $\lambda = \hbar\omega 2^{1/2} [-(1+\mu^2)^{1/2}, 0, 0, (1+\mu^2)^{1/2}]$, and the population of the target state must reach one. Applying the same rotation on the Hamiltonian we find:

$$\tilde{\mathcal{H}} = \frac{\hbar\omega}{\sqrt{2}} \begin{pmatrix} 0 & 2\mu & 0 & 0 \\ 2\mu & 0 & 0 & e^{i\phi_1} - e^{i\phi_2} \\ 0 & 0 & 0 & e^{i\phi_1} + e^{i\phi_2} \\ 0 & e^{-i\phi_1} - e^{-i\phi_2} & e^{-i\phi_1} + e^{-i\phi_2} & 0 \end{pmatrix} \quad (10)$$

So if $\phi_1 = \phi_2 + \pi$ one coupling in the Hamiltonian is null since $e^{i\phi_1} + e^{i\phi_2} = 0$ and the system is like a three states system, where the initial and the target state are coupled through a third state, this situation is represented by the Hamiltonian:

$$\tilde{\mathcal{H}} = \sqrt{2}\hbar\omega \begin{pmatrix} 0 & \mu & 0 & 0 \\ \mu & 0 & 0 & e^{i\phi} \\ 0 & 0 & 0 & 0 \\ 0 & e^{-i\phi} & 0 & 0 \end{pmatrix} \quad (11)$$

In this configuration a necessary condition to have a resonant evolution is to have the two modules of the coupling equals, so we must have $|\mu| = 1$. In a three state system, we already know which values of the energy of the central state gives a resonant evolution [5]. Then, we can modify the energy of the central state in the Hamiltonian and compute the inverse rotation. Doing this we find more complex Hamiltonians with resonant evolution. To give a clear example, we show on Fig. 4 the evolution of the population of the target state in the four different input configurations in the simplest case, i.e where $e=0$, $\mu=1$ and the two phases can take two values 0 or π

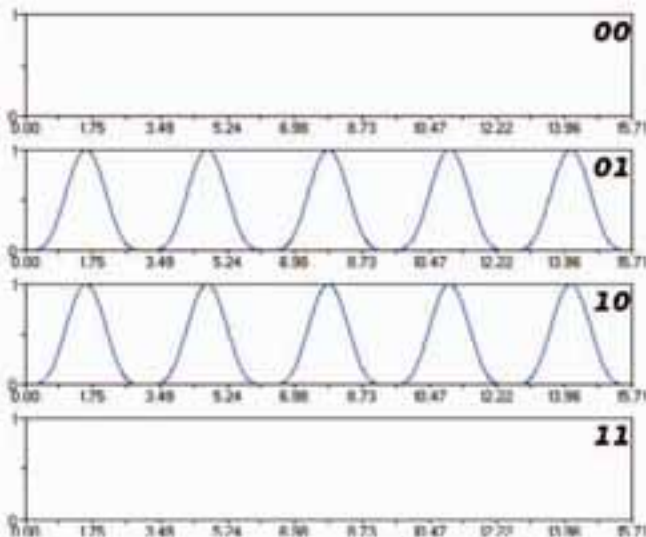


Figure 4: Evolution of the population of the target state for $\mu=1$, $e=0$, $\alpha = e^{i\phi_1}$, $\beta = e^{i\phi_2}$ and $\varphi_i = 0$ or π

The truth table of a XOR gate is satisfied since measuring at $t_m=(2k+1)\pi/(2\omega)$ the population of the target state will be one in the case of 01 and 10 input configurations and will be zero in the two other cases.

3.2 Encoding in the amplitude of the couplings:

In the second solution, α and β take only two values 0 or 1, like their classical logic gate input counterparts. The optimisation in that case is trickier. In the 00 configuration, since the target state is not coupled with the rest of the system, its population will remain equal to zero. In the 11 configuration the system, like in the previous section, is again in a perfect interference case, so the population of the target state will remain equal to zero too. We now have to tune the 01 and the 10 configurations in such a

way that the population of the target state reaches one at equal times. We first need to determine the value of μ . It can be shown that the only value of μ which allows the population of the target state to reach one is: $\mu = (1/2)^{1/2}$. We have then to find the values of e (a real quantity) which approach a periodic evolution.

$$\mathcal{H} = \hbar\omega \begin{pmatrix} 0 & \frac{1}{\sqrt{2}} & -\frac{1}{\sqrt{2}} & 0 \\ \frac{1}{\sqrt{2}} & e & 0 & \alpha \\ -\frac{1}{\sqrt{2}} & 0 & e & \beta \\ 0 & \alpha & \beta & 0 \end{pmatrix} \quad (12)$$

The eigenvalues of the Hamiltonian (12) are:

$$\lambda = \hbar\omega \frac{e}{2} \pm \hbar\omega \frac{\sqrt{e^2 + 2[(\alpha^2 + \beta^2 + 1) \pm \sqrt{(\alpha^2 + \beta^2)^2 - 4\alpha\beta + 1}]}}{2} \quad (13)$$

In the 01 case, the eigenvalues become:

$$\lambda_{01} = \hbar\omega \frac{e}{2} \pm \hbar\omega \frac{\sqrt{e^2 + 2(2 \pm \sqrt{2})}}{2} = \begin{cases} \lambda_1 = \hbar\omega \frac{e}{2} - \hbar\omega \frac{\sqrt{e^2 + 2(2 + \sqrt{2})}}{2} \\ \lambda_2 = \hbar\omega \frac{e}{2} - \hbar\omega \frac{\sqrt{e^2 + 2(2 - \sqrt{2})}}{2} \\ \lambda_3 = \hbar\omega \frac{e}{2} + \hbar\omega \frac{\sqrt{e^2 + 2(2 - \sqrt{2})}}{2} \\ \lambda_4 = \hbar\omega \frac{e}{2} + \hbar\omega \frac{\sqrt{e^2 + 2(2 + \sqrt{2})}}{2} \end{cases} \quad (14)$$

For a periodic evolution, the Hamiltonian must have four commensurate eigenvalues. We can tune easily the system to present at least two commensurate eigenvalues by finding the e values which lead to:

$$p(e) = \frac{\lambda_3(e)}{\lambda_2(e)} \in \mathbb{Q} \quad (15)$$

Solving (15) we find:

$$e = \pm(p-1) \sqrt{\frac{2-\sqrt{2}}{2p}} \quad (16)$$

where $p \in \mathbb{Q}$. We can then optimize p such that the four eigenvalues are almost commensurate. One simple example is $p = 42/10$ leading to:

$$e = \pm 3.2 \sqrt{\frac{2-\sqrt{2}}{8.4}} \quad (17)$$

which gives the eigenvalues: $\lambda \approx 1/\lambda_2[-3.6, -1, 4.2, 6.8]\hbar\omega$, and the evolution presented in Fig. 5 page 8. This evolution is quasi-periodic since λ_1 and λ_4 are not commensurate with λ_2 and λ_3 .

Like in the previous case, the truth table of a XOR gate is satisfied, since the population of the target state reaches almost one. For instance $P(t_m) > 90\%$ in the 01 and 10 configurations for k values as big as 10^3 , with:

$$t_{ms} = \frac{2k+1}{\omega} \frac{2\pi}{\sqrt{e^2 + 2(2+\sqrt{2})} - \sqrt{e^2 + 2(2-\sqrt{2})}} \approx \frac{2k+1}{\omega} 4.57 \quad (18)$$

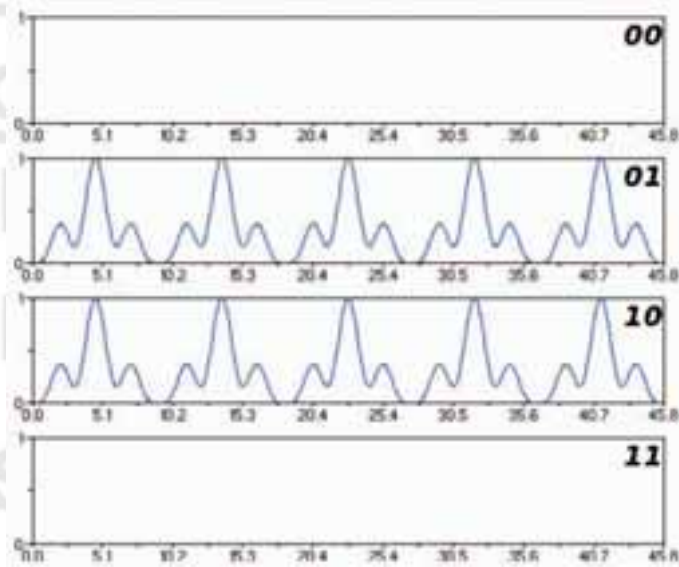


Figure 5: Evolution of the population of the target state for $\mu = 2^{-1/2}$, $e \sim 0.85$, $\alpha = 0$ or 1 and $\beta = 0$ or 1

4. Study of the trajectory of a N state system by the Majorana representation

There are several ways to represent the evolution of a quantum system. For two-state systems, which are ubiquitous in physical systems, the most useful representation is the so-called Bloch representation where the quantum state is represented as a point on a sphere. In this case, the Hamiltonian is even displayed as a vector, threading the sphere around which the representative point precesses, in full analogy with a spin $1/2$ precessing around a magnetic field.

For N -level quantum systems, the situation is more complex. An unambiguous quantum state representation is still possible with $N-1$ points on a sphere, by considering the old, but poorly known, Majorana high spin representation. But in this case, as discussed below, the nature of the quantum state evolution can be rather complex on the sphere.

For a N -level quantum system, we associate to the state $|\Psi\rangle = \{a_1, a_2, \dots, a_N\}$ a polynomial of degree $N-1$ defined as:

$$P_\psi = \sum_{j=0}^{N-1} (-1)^j \binom{d}{j} a_{j+1} z^j = a_{N-1} \prod_{j=1}^{N-1} (z - z_j)$$

In this way the state $|\Psi\rangle$ can be associated to the $N-1$ roots of the equation $P_\psi = 0$. These roots z_i ($i=1, \dots, N-1$) are complex numbers, which can be represented on a sphere by means of an inverse stereographic projection:

Advertisement

NANOTECHNOLOGY

Raith

INNOVATION FROM A WORLD LEADER IN ELECTRON BEAM LITHOGRAPHY AND SEMICONDUCTOR NAVIGATION SOLUTIONS

Electron beam lithography solutions

for your nano science center, university institute, educational facility



RAITH150

Ultra high resolution electron beam lithography and metrology tool



e_LINE

Ultra high resolution electron beam lithography and nano engineering workstation

RAITH50

Universal electron beam lithography tool

www.raith.com

Raith GmbH - Hauptstr. 44227 Dortmund - Germany - phone +49 (0)231 / 975 000-0 - fax +49 (0)231 / 975 000-5 - email postmaster@raith.de

$$(x(z_i), y(z_i), z(z_i)) = \frac{1}{1 + |z_i|^2} \{\Re(z_i), \Im(z_i), 1 - |z_i|^2\} \quad (19)$$

Therefore, the Majorana representation allows to describe a quantum state (and its evolution) with $N-1$ points on the sphere.

To show how the Majorana representation can be useful in describing the quantum evolution, we analyse in details the two logical gates constructed in section 3 in both phase and amplitude cases. Since we are dealing with a 4-level system, the quantum state is described by three points on the Majorana sphere.

The initial state, with respect to the local basis used in (5), is $|\Psi_0\rangle = \{1,0,0,0\}$ while the target state is $|\Psi_{\text{target}}\rangle = \{0,0,0,1\}$. Then, starting from $|\Psi_0\rangle$, if after a defined time interval the system ends up in the target state $|\Psi_{\text{target}}\rangle$, the logical 1 value is assigned to the computation; if it does not end up in $|\Psi_{\text{target}}\rangle$ the logical 0 is assigned.

In the Majorana representation these states correspond to the (three) points gathered at the south pole ($|\Psi_0\rangle \rightarrow (0,0,-1)$) or at the north pole ($|\Psi_{\text{target}}\rangle \rightarrow (0,0,1)$). Then, for the studied gate, we expect the system to reach the final state $|\Psi_{\text{target}}\rangle$ if the logical input in the Hamiltonian (6) are (1,0) or (0,1). In terms of evolution on the Majorana sphere, we expect the three points to evolve from the south pole to the north pole, as can be seen in **Fig. 6**.

For the logical 0 output (logical (0,0) and (1,1) inputs), the points never reach (simultaneously) the north pole, **Fig. 7**. Note that, in these cases, only two curves are shown meaning that the third point remains at the south pole during all the evolution. We have further degree of freedom with the Majorana representation in order to simplify or to clarify some aspects of the evolution. Particularly useful is the possibility to describe the evolution in the basis which diagonalise the Hamiltonian (5). In this case the initial and the final states no more sit at the poles, but the evolution on the Majorana sphere is simplified.

These simple examples show that the Majorana representation can be useful to describe the evolution of a quantum system. The possibility to visualise the quantum state on a sphere allows to clarify some features that in other cases should be more difficult to grasp. For example, in case of non-periodic evolution, the corresponding curves of the points on the Majorana sphere are not closed, as can be readily seen in this representation.

5. Performance of the XOR gate in phase and amplitude implantation

What is the most efficient implementation of an XOR gate in a QHC architecture? To answer this question we need to find a criterion which allows us to quantify the efficiency of those two approaches. One good solution is to compare the energy required for the computation. The initial non-stationary state presents a higher energy, $\langle \Psi_0 | \mathcal{H} | \Psi_0 \rangle$ than the ground state energy E_0 of the system. Therefore the energy required for the computation is given by:

$$\Delta E = \langle \psi_0 | \mathcal{H} | \psi_0 \rangle - E_0 \quad (20)$$

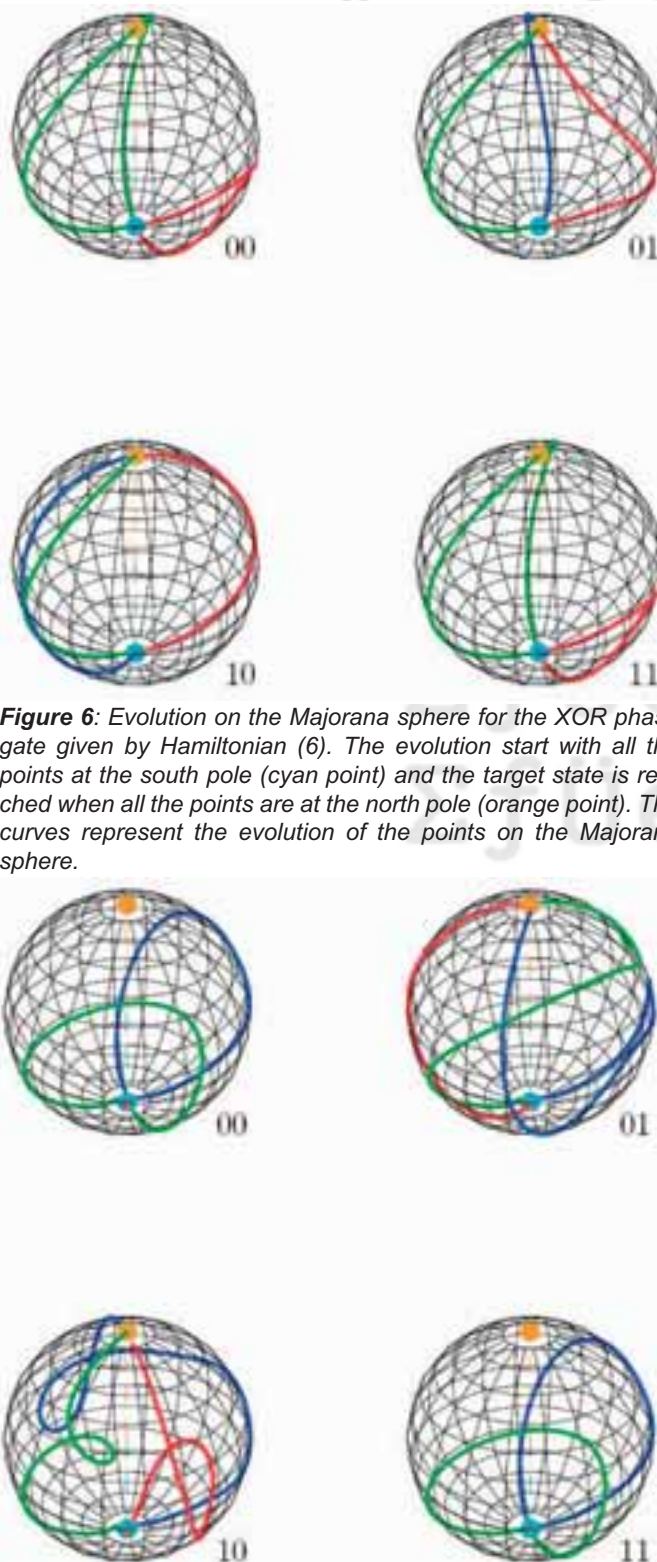


Figure 6: Evolution on the Majorana sphere for the XOR phase gate given by Hamiltonian (6). The evolution start with all the points at the south pole (cyan point) and the target state is reached when all the points are at the north pole (orange point). The curves represent the evolution of the points on the Majorana sphere.

Figure 7: Evolution on the Majorana sphere for the XOR amplitude gate given by Hamiltonian (12). The evolution start with all the points at the south pole (cyan point) and the target state is reached when all the points are at the north pole (orange point). The curves represent the evolution of the points on the Majorana sphere.

For the same computation time we can then estimate how much energy is required in the two versions in the different input configurations

The time-energy inequality $\Delta E \Delta t \geq \hbar$ can also be used as a criterion to compare the efficiency of the logic gates.

We have seen that the computation time for the XOR phase gate is $t_m = 1/2\pi\hbar$. We have now to force the amplitude-

XOR gate to have the same computation time. We just have to multiply its Hamiltonian by the ratio of the two computation times. Since the initial state is not the same on the eigenbasis for all the different configurations, the

Logical Input	E_{phase}	E_{Amp}
00	$\sqrt{2}h\omega$	$1.92h\omega$
01	$2h\omega$	$2.75h\omega$
10	$2h\omega$	$2.75h\omega$
11	$\sqrt{2}h\omega$	$3.05h\omega$

Figure 8: Energy required to perform the computation in the same time for both phase and amplitude implantation

energy required is not the same. Following this approach we find the results shown in **Fig. 8**.

The performance of the two implementations are quite the same even if the phase implementation is a little better in terms of energy, especially in the 00 and 01 configurations. Another interesting point is the encoding of the information in the system. In the classical case, the words used here are quite easy since they contain only two binary letters. As soon as we change the two parameters

cWord	qWord							
00	-0.663	0.000	0.845	1.508	0.833	0.000	0.000	-0.552
01	-0.950	-0.264	1.109	1.795	0.571	-0.635	0.310	-0.416
10	-0.950	-0.264	1.109	1.795	-0.571	-0.635	0.310	-0.416
11	-1.053	-0.663	1.508	1.898	0.000	-0.833	0.552	0.000

Figure 9: Encoding of the input data to go from a classical word (cWord) to a quantum word (qWord)

in the Hamiltonian we change its four eigenvalues, the four eigenvectors, and the development of the initial state in the eigenbasis. So eight real numbers are changed to encode the XOR four possible input configurations. Therefore this quantum input word contains in fact the four eigenvalues and the four coefficients of the initial state on the eigenvectors (eight in the generic case where eigenvectors may have complex coordinates). Following this procedure for the XOR amplitude gate we find the result shown in **Fig. 9**.

In the tabular 9 the four first numbers of the quantum word are the eigenvalues of the system and the last four are the coefficients of the initial state on the eigenbasis. Even if we still need new tools to understand better this translation process from the classic to the quantum word, we clearly see here that the classical logic input word is turned into a complex quantum word.

6. Conclusion

We have shown here how to design an XOR gate taking in account only the intrinsic quantum evolution of a three state system.

Advertisement



www.schaefer-tec.com

SCHAEFER Techniques
1, rue du Ruisseau Blanc
Centre d'Activité de Lunezy
F-91620 Nozay

Telephon: +33 (0) 1 64 49 63 50
Telefax: +33 (0) 1 69 01 12 05
E-Mail: info@schaefer-tech.com
Web: www.schaefer-tech.com

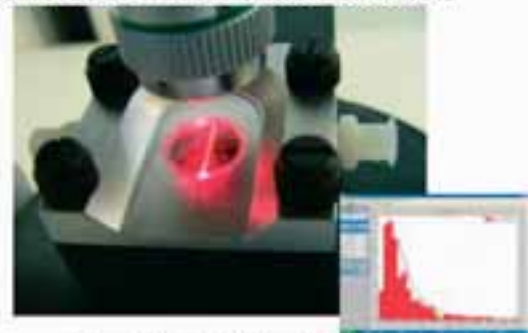
NEW Instruments for New Challenges !

Scanning Probe Microscopes Modular & Compact System



Nanosurf, easyScan 2

Nanoparticle Analysis Individual & Real Time Detection



NanoSight, Halo LM10

We also represent the following companies, please contact us for further information :

- RHK for UHV STM/AFM and Cryogenic SPM
- QUESANT for AFM and STM
- MIKROMASCH for AFM tips and gratings
- KRATOS for XPS instrumentation
- OCI for LEED and AES
- FOGALE for optical Probers
- ALICONA for InfiniteFocus Microscope and MeX
- HASTINGS for Vacuum and Gas Flow measurement
- HUNTINGTON for Vacuum Components

... and many other products in the field of Vacuum, Magnetism, Thin Film and Cryogenics

The criteria of fidelity impose the system to present a periodical evolution and then commensurable eigenvalues in each input configurations. Even if finding a $N \times N$ Hamiltonian with commensurable eigenvalues is an easy task, finding an Hamiltonian $\mathcal{H}(\theta_1, \theta_2, \dots, \theta_p)$, depending of p binary parameters with commensurable eigenvalues in each 2^p input configurations is much more complex problem. We can get around this difficulty finding quasi-period evolution of the population of the target state. Those kind of evolutions are able to reach almost one and the measurement can be performed during many quasi-period of the evolution. However this periodicity problem plus the difficulty to access the exact wave function of the system at a very specific time leads, in the context of Pico-Inside, to design logic gates with others measurement process. One of those process could be to encode the result of the computation in the frequency of the evolution of the population of the target state since we know that this frequency is related to the intensity of tunnelling current through the system.

The use of the Majorana representation provides a geometrical representation of the evolution of a general N -states system without any loss of information. Consequently it is a good tool to follow the evolution and understand the control of its trajectory by its own Hamiltonian. In Pico-Inside we are now studying bigger system to design more complex quantum Hamiltonian logic gates.

References

- [1] J. Furjasek, N. Cerf, I. Duchemin, C. Joachim. *Hamiltonian Logic Gates: computing inside a molecule*. **International Journal of Nanoscience** **24**, 161-172, 2005
- [2] I. Duchemin, C. Joachim. *A quantum digital half adder inside a single molecule*. **Chem. Phys. Letter**, **406**, 167-172, 2005
- [3] C. Joachim. *The diving Power of the superposition principle for molecules-machines*. **J. Phys. Condensed Matter**, **18**, S1935-S1942, 2006
- [4] E. Majorana. *Atomi orientati in campo magnetico variabile*. **II Nuovo Cimento**, **9**, 1932
- [5] P. Sautet, C. Joachim. *The switching ability of a three-level tight-binding system: the isolated and embedded case*. **J. Phys. C: Solid State Physics**, **21**, 3939-3957, 1988.

Electronic control inside a single molecule on semiconductor surfaces

A. Bellec, F. Chiaravalloti, G. Dujardin and D. Riedel
Laboratoire de Photophysique Moléculaire
Bâtiment 210, Université Paris-Sud
91405 Orsay, France

Keywords: STM, low temperature, semiconductor, biphenyl, dynamics, transport

1. Introduction

The PicoInside project aims at exploiting the unique quantum, i.e. electronic and dynamical, properties of a single molecule to achieve computing inside the molecule. As recently demonstrated, the picometer precision required to contact and to control the operation of a single molecule can be best achieved by using low temperature scanning

tunneling microscopy (LT-STM) [1-3]. The choice of the substrate for anchoring the molecule is also crucial. Semiconductor substrates have a number of advantages over other types of substrates. They have a bulk band gap (from 1.1 eV for silicon to 5.5 eV for diamond) which enables to electronically decouple the molecule from the substrate. However, semiconductors may have surface states whose energy lies within the bulk band gap. Electrical surface conductivity through these surface states can modify, at least partially, the electronic decoupling of the molecule. It can also be turned into an interesting method to electrically contact a single molecule, provided the surface is adequately nanostructured. However, surface conductivity can be suppressed either by freezing some electronic conduction channels at low temperature [4] or by passivating the semiconductor surface with insulating thin layers as will be shown in part III. Another advantage of semiconductor surfaces that will be illustrated in part II is the ability to dope the substrate with different types of dopants (n or p). This allows to tune the dynamics of adsorbed molecules and may find important applications for high precision positioning of individual molecules.

2. Picometer-scale electronic control of molecular dynamics inside a single molecule

To achieve the computing inside a single molecule, it is necessary to control at the picometer-scale the dynamics of the molecule. This will provide the way to control the inputs of the logic gate calculation through the local change of molecular conformation.

Recently, it has been demonstrated that a single biphenyl molecule adsorbed at room temperature on a Si(100) surface behaves as a bistable molecule at low temperature (5K) [3]. The underlying physics describing the dynamic of such a molecular device is governed by a multi-dimensional surface potential that should be subtly influenced by the interaction between the molecule and its atomic scale surrounding. Powering and controlling the operation of this bistable molecule on a semiconductor surface can be done by electronic excitation with the tip of a low temperature STM [3]. Here, we demonstrate that the presence or not of just one hydrogen atom in the vicinity of the molecule dramatically modifies the molecular dynamics of the bistable biphenyl. We further show that the type of dopant (n or p) of the silicon substrate can also strongly influence the dynamics of the biphenyl molecule. Whereas, this extreme sensitivity of the molecular dynamics to the atomic-scale surrounding may appear at first as an actual difficulty, we will see that it may be turned into an advantage to further control the dynamics of a single molecule.

2.1 Mastering the molecular dynamics of a single molecule by single atom manipulation

In its bistable configuration, the biphenyl molecule has two equivalent stable positions, S_1 and S_2 , as shown in the STM topographies of **Fig. 1 page 12**. The biphenyl molecule is seen as a pair of bright features representing the two phenyl rings of the molecule. This bistable adsorption

configuration consists of one phenyl ring lying parallel to the surface and attached to a silicon dimer in the so called "butterfly" configuration through two C-Si chemical bonds [5]. This phenyl ring is centered over the silicon dimer row. The second phenyl ring, perpendicular to the surface, is attached to a silicon atom through a single C-Si chemical bond. This is the result of a dissociative adsorption of the second phenyl ring where one hydrogen atom of the phenyl ring is adsorbed into the Si atom of the dimer as shown in Fig. 1.

As previously reported [3], the reversible switching of the

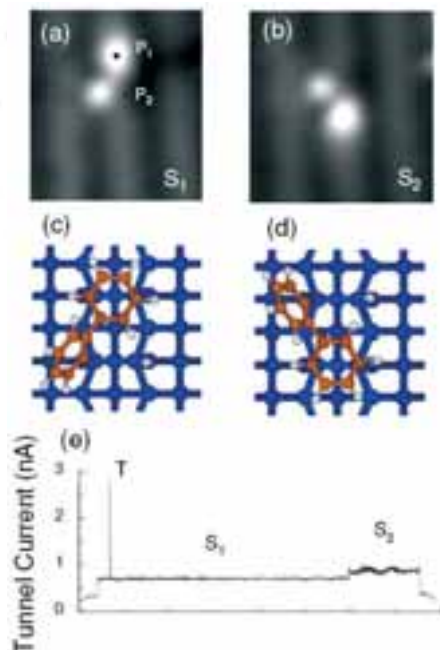


Figure 1: (a) (23 Å by 23 Å) topography of a single biphenyl molecule in the stable configuration S_1 . The dots indicate the STM tip position (P_1 and P_2) where the negative bias pulse is applied. (b) Same as (a) after the surface pulse. The molecule has switched to its second stable configuration S_2 . (c) to (e) Three typical tunnel current curves recorded during negative bias pulses at P_2 ($V_S = -3V$, $t = 8s$) give insight into the dynamics of the molecular switch.

molecule from S_1 to S_2 can be activated through resonant electronic excitation by positioning the STM tip at different positions inside the molecule (for example positions P_1 and P_2 in Fig.1) and applying a pulse voltage ($V_S = -3.5V$) on the surface. Recording the tunnel current during the pulse voltage enables a detailed investigation of the dynamics of the molecule as a function of the time of excitation. The tunnel current curve in Fig. 1e, recorded with the STM tip in position P_2 , illustrates an example of the molecular movements. The small step corresponds to the switching of the molecule from S_1 to S_2 . The tunnel current curve shows also a very narrow peak (T) that is related to the brief passage through a transient molecular state T [3]. The $S_1 \rightarrow S_2$ switching requires one of the molecular phenyl rings (called the mobile phenyl ring) to break two Si-C bonds in its butterfly position, to move over the Si-H bond and to make two new Si-C bonds to recover its butterfly position at the second silicon dimer site. In the meantime, the other molecular phenyl ring (called the fixed phenyl ring) is expected to rotate around its single

Si-C bond. It follows that the Si-H bond behaves as an obstacle to the operation of the bistable molecule since a part of the molecule has to pass over the hydrogen atom for switching to occur. Therefore, we decided to desorb this hydrogen atom with the STM tip in order to explore the resulting dynamics of the molecule. The desorption of hydrogen has been performed by using a negative surface voltage $V_S = -4V$ with the STM tip on top of the hydrogen atom (position P_2 in Fig. 1). The desorption of the hydrogen atom after an excitation time t_d is clearly evidenced in the tunnel current curve of Fig. 2.

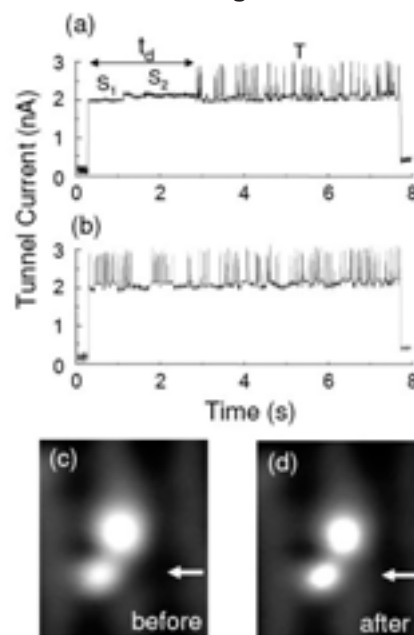


Figure 2: (a) Tunnel current during a negative bias pulse at P_2 ($V_S = -4 V$, $t = 8s$). Desorption of the hydrogen atom occurs at time t_d . (b) Tunnel current during a negative bias pulse ($V_S = -4 V$, $t = 8s$) after hydrogen desorption. (c) and (d) 20 Å by 20 Å STM topographies of the biphenyl molecule before and after the hydrogen desorption. The arrow indicates the area where the hydrogen atom has been removed leading to a slightly higher local density of states.

Indeed, before time t_d , the molecule switches only once from S_1 to S_2 . After a time t_d , the molecule has a completely different behaviour. It switches much more often between the S_1 , S_2 and T states. We have found that the switching yields for excitation pulses of $-3.5 V$ are increased after hydrogen desorption by a factor 3 to 50 depending on the excitation position and the molecular movement ($S_1 \rightarrow S_2$ or $S_1 \rightarrow T$). Another interesting consequence of the hydrogen desorption is that the molecule can now be switched (by applying a pulse voltage ($V_S = -3.5V$)) into any of the four molecular configurations imaged in Fig. 3 page 13. The S_1 and S_2 states are the same as before hydrogen desorption, whereas two new states (S_3 and S_4) of the molecule can be imaged with the STM. The occurrence of the four stable states (S_1 to S_4) and the transient states (T) can be seen in the tunnel current curve (Fig. 3e). Compared to the operation of the bistable molecule, where the biphenyl molecule could be switched only between two stable states (S_1 and S_2), the operation of the multistable molecule after hydrogen desorption is

much more complicated since it can now be switched between four stable positions (S_1 , S_2 , S_3 and S_4). So far, we have found the switching of the multistable molecule to be random. A sequence of switching events is shown in **Fig. 3**. Nevertheless, further studies as a function of the pulse voltage and the position of the STM tip are required for a more complete understanding of the multistable molecule operation. These results reveal that a precise control of each atom position around the molecule needs to be achieved if a quantitative operation of a molecular device is required. This single atom sensitivity can give rise to very interesting perspectives for engineering the performance of a molecular device. One can expect being able to control, by single atom manipulation, not only the operation of a molecular device but moreover its intrinsic performance (e.g. the switching frequency or the number of stable states).

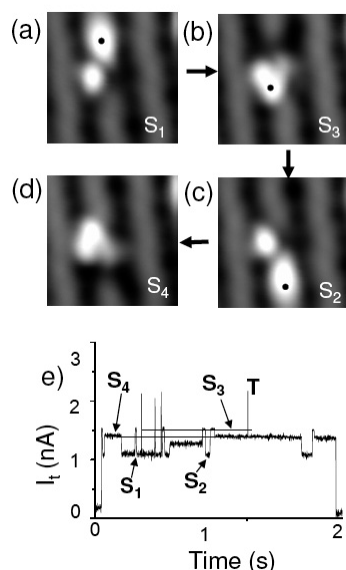


Figure 3: (23 Å by 23 Å) STM topographies of the four stable configurations of the biphenyl molecule after its H atom desorption. (a) and (c) depict the S_1 and S_2 configurations respectively. (b) and (d) show the two new stable S_3 and S_4 configurations. The series a) to d) (following the arrows) is a succession of molecular manipulations of the multistable molecule using negative surface pulses ($V_s = -3.0$ V) applied at the indicated black dots.

2.2 The role of the dopant in silicon on the dynamics of a single adsorbed molecule

We have investigated the role of the type of dopant in silicon on the properties of the bistable biphenyl molecule, in particular on its molecular dynamics. The STM topographies of the bistable biphenyl molecule (for any surface voltage in the -2V to +2V range) are similar whatever the substrate type of dopant (see **Fig. 4**) although the STM imaging of the Si(100) surface itself is known to depend on the type of dopant [6]. However, the molecular dynamics of the bistable molecule as probed by recording the tunnel current during the pulse voltage is markedly different for p-doped and n-doped silicon (see **Fig. 4c and 4d**). Numerous peaks are observed in the tunnel current curve of the p-doped sample for time $t < t_{exc}$, t_{exc} being the time of excitation before the molecule switches from S_1 to S_2 .

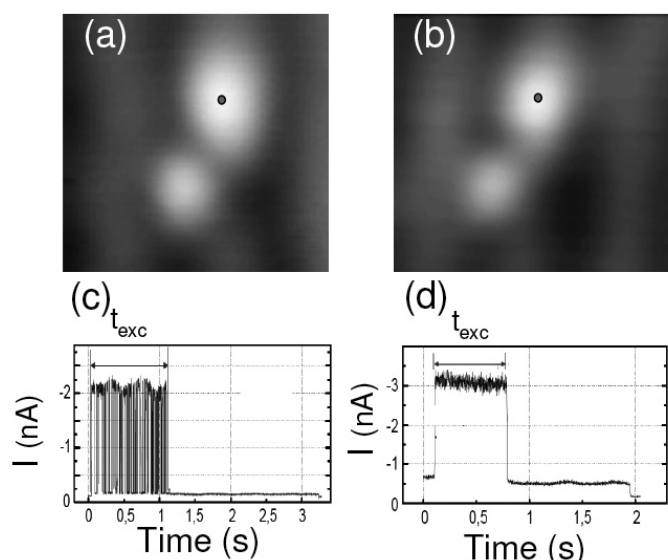


Figure 4: a) and b) are the STM topographies ($V_s = -2V$, $I = 0.2$ nA) of a single biphenyl molecule in the S_1 conformation on a p-doped and a n-doped Si(100) surface respectively. c) and d) are the tunnel current as a function of time during the pulse voltage for a p-doped and n-doped Si(100) surface respectively. The drop of the tunnel current at time t_{exc} is due to the switching of the molecule from S_1 to S_2 .

These peaks correspond to the movement of the molecule into a transient molecular configuration T which is too unstable to be imaged with the STM. From the width of the peaks in **Fig. 4c**, the time the molecule adsorbed on the p-doped silicon spends in the T transient state has been found to be in the range 1-100 ms depending on the tunnel current and surface pulse voltage. Surprisingly, no evidence of the transient T molecular configuration could be observed with n-doped silicon (see **Fig. 4d**) whatever the tunnel current and surface pulse voltage. Considering the bandwidth of our tunnel current detection (below 1.3 KHz), we deduce that the time the molecule spends in the transient T state is at least 2 orders of magnitude smaller for n-doped than for p-doped silicon. The unchanged stability of the S_1 and S_2 biphenyl molecular configurations and the increased instability of the T configuration with n-doped silicon is believed to be related to the negative charging of surface states [7]. This induces a surface electric field which is likely to influence the stability and the dynamics of the molecule in its T configuration. Indeed, in the S_1 and S_2 configurations, both phenyl rings of the biphenyl molecule are considered to be strongly chemisorbed to the surface. In the T transient configuration only one phenyl ring (fixed phenyl ring) is chemically bound to the surface through a Si-C bond. The second phenyl ring (mobile phenyl ring) is not chemically bound to the surface and will therefore undergo the influence of the surface electric field. This effect is expected to be markedly increased by the negative charge on the mobile phenyl ring [8]. The repulsive interaction between this negative charge located on the mobile phenyl ring and the negative surface charge explains the increased instability of the T configuration of the biphenyl molecule with n-doped silicon. On p-doped silicon, the charge of surface states is

somehow more controversial. A downward band bending, associated to a positive charging of surface states, has been detected at low temperature on p-doped substrates but was attributed to a small density of surface states which could originate from defects [8]. Since our surfaces have a very low density of defects, the surface states on p-doped substrates are likely to be neutral. In any case, the T configuration is expected to be more stable on p-doped silicon than on n-doped samples as it is observed experimentally.

In addition of its fundamental interest, this new phenomenon, which enables to select the dynamics and the adsorption stability of individual molecules by tuning the type of dopant of a silicon surface, may have very important applications. By using the semiconductor industry processing techniques, one can pattern silicon surface areas of different types of doping (n and p) [7]. This could be used, for example, to adsorb molecules at selected locations or to guide the movement of molecules along selected paths across a surface. From this, new methods for accurately positioning individual molecules can be anticipated.

3. Electrical contact of a single molecule

The multiple electrical contact of a single molecule is actually one of the main problems to be solved in Picoinside to demonstrate the computing inside the molecule. For that purpose, two principal problems need to be solved. Firstly, the molecule needs to be electronically isolated from the substrate. This can be best achieved by using insulating layers (see Fig. 5) thin enough (thickness of the order of 1 nm) to allow STM imaging by tunneling through the molecule and the insulating layer. The advantage of an insulating layer grown on a semiconductor substrate com-

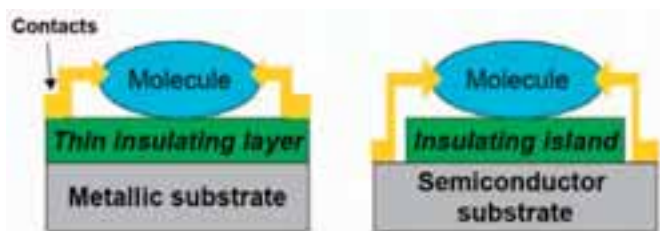


Figure 5: Schematics of a single molecule adsorbed on an insulating layer with a metallic (left) and semiconductor (right) substrate.

pared to a metallic substrate is that the insulating layer is expected to suppress all the surface conductive channels having energies within the bulk band gap. By this way, the electronic isolation of the molecule is complete for all energies lying within the bulk band gap whereas some weak electronic coupling is always present in the case of the metallic substrate. Another advantage of semiconductor substrates is that the electrodes contacting the molecule can be built directly on the semiconductor substrate. Indeed, growing conducting electrodes is a priori much easier on semiconductors than on insulators due to the stronger interactions between adsorbates and semiconductor surfaces as compared to insulator surfaces. The second problem to be solved for electrically contacting a single molecule is to control, with atomic-scale precision, the contact between the molecule and the electrodes. Building conducting atomic lines by atom manipulation with the STM is probably the most controlled way to contact a single molecule. We will illustrate this method in the case of the hydrogenated silicon surface.

Advertisement

NanoMEGAS has been created in 2004 by a team of scientists with expertise in electron crystallography



NanoMEGAS
Advanced Tools for electron diffraction

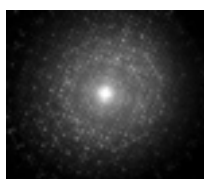
Our products are dedicated to help the TEM user (100-400 kv) to find in an easy way the true structure (crystal parameters, symmetry and atomic positions) of nanomaterials that are otherwise impossible to determine by X-ray diffractometry or high resolution TEM microscopy.

Our product “**spinning star**” takes control of the electron beam in a TEM and performs precession of a beam (Vincent- Midgley technique) in a way that one can obtain almost “kinematical” diffraction patterns.

A special dedicated software (**ELD-Emap**) can read and measure in automatic way intensities of ED patterns obtained with “**spinning star**”.

Spinning Star: Automatic Determination of Crystal Symmetry (K3Nb12O31F crystal)

PRECESSION OFF
1786 reflexions



PRECESSION ON
3367 reflexions



NanoMEGAS SPRL

Boulevard Edmond Machtens 79; B-1080 Brussels (Belgium)
Email: info@nanomegas.com / <http://www.nanomegas.com>

3.1 Thin insulating layer on a semiconductor substrate; the case of CaF_2 on $\text{Si}(100)$

In recent years, there have been a number of studies for investigating the growth of insulating layers on metallic surfaces with the aim to deposit molecules on top of them for molecular self-assembling or molecular electronics purposes [1,9]. Similar studies on semiconductor surfaces are very scarce in the literature. Limitations are related to the necessary matching between the crystalline structure of the layer and that of the semiconductor substrate. So far, two main systems have emerged: (i) Oxide layers on silicon. Initially motivated by the fabrication of high K gate oxides for CMOS devices, oxide layers have been recently assigned much more functionalities (sensor, actuator). As a result, an integrated multi-function oxide electronics is now emerging. Although, crystalline structures of such oxide layers on silicon have been demonstrated [10], the quality of their surface at the atomic-scale has not yet been tested, (ii) CaF_2 layers on silicon. Calcium fluoride layers have been successfully grown on both $\text{Si}(111)$ and $\text{Si}(100)$ and their structure analysed by synchrotron radiation based techniques and atomic force microscopy (AFM) [11,12]. However, the atomic-scale structure and electronic properties of these calcium fluoride layer surfaces have not yet been studied.

We have investigated the growth, the atomic-scale structure and the electronic properties of thin calcium fluoride layers on $\text{Si}(100)$ surfaces by using the low temperature (5K) STM. CaF_2 molecules sublimated from CaF_2 crystals have been deposited under UHV on highly n-doped $\text{Si}(100)$ substrates maintained at 650°C . After cooling down to 5K, the resulting layers have been imaged with the STM as shown in Fig. 6 for low coverage (< 0.3 ML) and higher coverage (1.2 ML). At low coverage (Fig. 6a), one dimension (1D) and two dimension (2D) islands with regular structure are observed. The 1D structures enable to distinguish the unit cell. At higher coverage (Fig. 6b), islands with the same structure as at low coverage cover most of the sample surface (darkest areas in Fig. 6b). In addition, very long stripes (hundreds of nm) having very few defects are observed. It is believed that the stripes are grown on top of the first layer seen as islands in Fig. 6a. STM I(V) spectroscopy of the stripes (not shown here) has yielded a surface gap of about 4 eV. These preliminary results open interesting perspectives. Within the energy range from -1.5 eV to +2.5 eV, molecules adsorbed on top of (or between) the stripes should be electronically decoupled from the silicon substrate. Furthermore, the 1D structure of the stripes might allow the self-organisation of molecular lines or alternatively of atomic lines along the calcium fluoride stripes.

3.2 Thin insulating layer on a semiconductor substrate; the case of hydrogenated $\text{Si}(100)$

The simplest method to insulate the surface of silicon is to passivate its surface by adsorbing hydrogen atoms on the silicon dangling bonds. By this way, surface state conductivity within the bulk band gap is expected to be suppressed. This has been quantitatively demonstrated by Doumergue et al. [13] who calculated the electron trans-

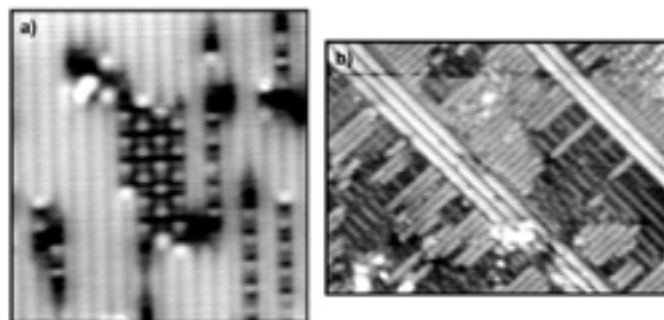


Figure 6: Low temperature STM topographies of CaF_2 adsorbed on $\text{Si}(100)$. a) $29 \times 29 \text{ nm}^2$, $V_S = 1.8 \text{ V}$, $I = 61 \text{ pA}$, coverage ($< 0.3 \text{ ML}$). b) $23 \times 31 \text{ nm}^2$, $V_S = -2 \text{ V}$, $I = 160 \text{ pA}$, coverage 1.2 ML.

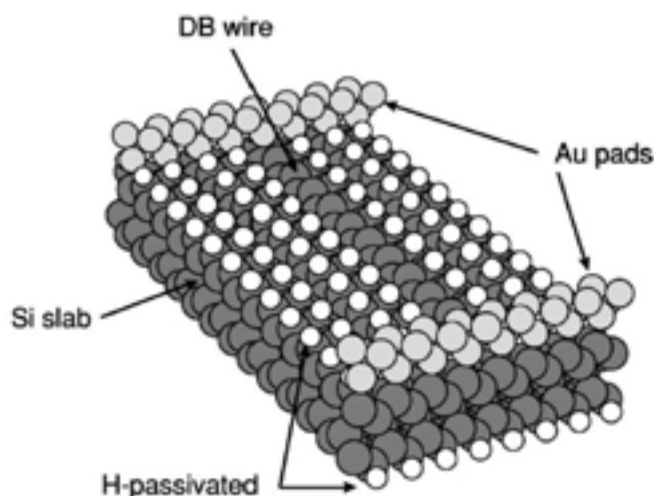


Figure 7: Schematics of a Si dangling bond (DB) wire connected to two Au pads on a $\text{Si}(100)$ surface, taken from [13].

mission through various types of atomic lines on the hydrogenated $\text{Si}(100)$ surface (see Fig. 7). In the case of the perfect $\text{Si}(100)-(2 \times 1): \text{H}$ surface, the transmission has been found to strongly exponentially decrease as a function of the inter-pads distance. The calculated inverse decay length was $\gamma = 0.41 \text{ \AA}^{-1}$, i.e. smaller than for tunneling through vacuum ($\gamma = 2.21 \text{ \AA}^{-1}$). When a silicon line is de-passivated (hydrogen desorbed), the resulting silicon dangling bonds form a metallic wire whose electron transmission is constant as a function of the inter-pads distance (see Fig. 7). However, it has been demonstrated that the silicon dangling bond line is not stable and undergoes a Peierls-like distortion [14]. This removes the metallic character of the atomic line and results in opening a small gap of 0.2 eV. The electron transmission through this distorted atomic line has been found to slightly decrease as a function of the inter-pads distance with an inverse decay length of $\gamma = 0.09 \text{ \AA}^{-1}$ [13]. Experimentally measuring these electron transmissions as described in Fig. 7 is not possible due to the difficulty in fabricating the two pads with the appropriate atomic-scale precision. We have recently initiated a different method to measure these electron transmissions. This is illustrated in Fig. 8 page 16. Atomic lines of hydrogenated silicon atoms can be easily selected either parallel or perpendicular to the silicon dimer rows. Atomic lines of deshydrogenated silicon dan-

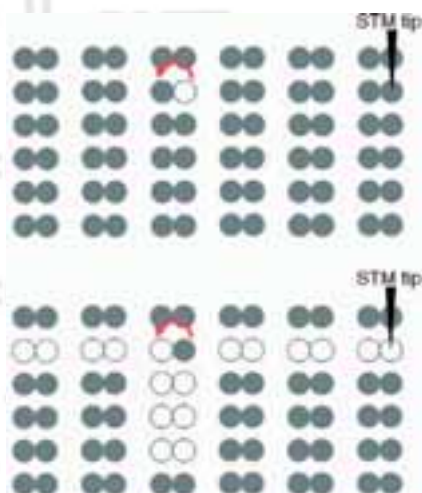


Figure 8: Schematics of atomic lines on a Si(100) surface. The grey circles are the hydrogenated silicon atoms. The white circles are the silicon dangling bonds. The red arrow indicates the atom switch. The STM tip position for injection of charges is also indicated. The surface is fully hydrogenated (top) or partially deshydrogenated (bottom).

gling bonds can be precisely produced by selectively desorbing hydrogen atoms one by one through electron excitation with the STM tip [15]. The method for measuring the electron transmission (see Fig. 8) consists in using the STM tip as one of the two pads at one end of the atomic line. At the other end, a silicon dangling bond atom switch is placed to detect the transmitted charges. Indeed, it is known that a silicon dangling bond, produced by desorbing one hydrogen atom from an hydrogenated silicon dimer, behaves as an atom switch which can be activated by charging [16]. The atom switch is then working as a charge detector at the second end of the atomic line (see Fig. 8). Charges injected at one end of the atomic line with the STM tip are transmitted through the atomic line and then activate the atom switch at the other end. The yield for activating the atom switch (probability of switching per injected charge) can be measured for various types (hydrogenated or dangling bonds), lengths and orientations (relative to the dimer row direction) of the atomic line. The STM topography of the hydrogenated Si(100) surface

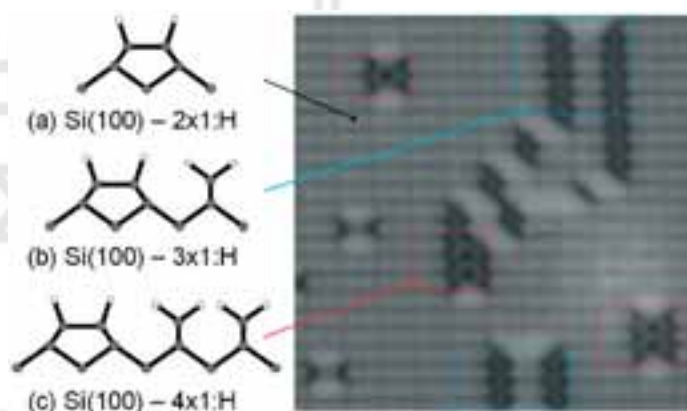


Figure 9: Low temperature (5K) STM topography of the hydrogenated Si(100) surface ($8.5 \times 8.5 \text{ nm}^2$, $V_S = 1.7 \text{ V}$, $I = 110 \text{ pA}$) showing the various surface reconstructions.

recorded at 5K is shown in Fig. 9. Several surface reconstructions are seen. The 2x1 and 3x1 reconstructions have been previously observed at room temperature. However, a new 4x1 reconstruction which has never been observed at room temperature is seen at 5K. A tentative structure for this new reconstruction is given in Fig. 9. For the fabrication of the silicon dangling bond lines, we have been working on the 2x1 reconstructed areas. The desorption of individual hydrogen atoms with the STM tip has been performed as previously described [15] by locating the STM tip on top of the chosen hydrogen atom, opening the feedback loop and applying a surface pulse voltage of +2.5 V. The result is shown in Fig. 10 where the silicon dangling bond is seen as a bright protusion in the STM topography.

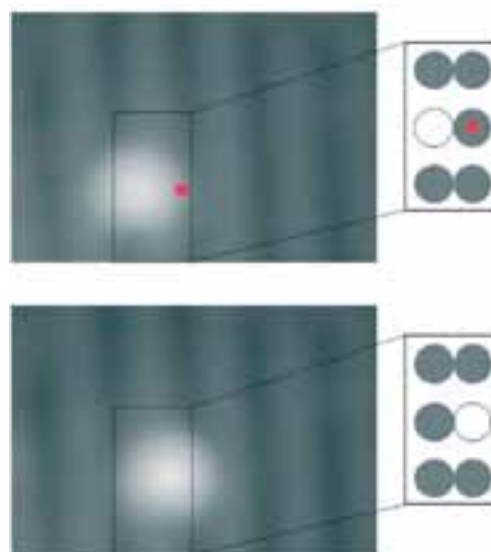


Figure 10: Low temperature STM topographies ($4 \times 2.75 \text{ nm}^2$, $V_S = -1.7 \text{ V}$, $I = 69 \text{ pA}$) showing the atom switch. Initially the silicon dangling bond (white circle) is on the left side of the silicon dimer row (top STM topography). Then the STM tip is positioned on top of the hydrogen atom (red circle) and a negative surface voltage pulse is applied (-2.5 V). As a result, the silicon dangling bond has been switched to the right side of the silicon row (bottom STM topography).

We have first tested the activation of the atomic switch made of the single dangling bond by locating the STM tip directly on top of the neighbouring hydrogen atom and applying a negative surface voltage pulse. The atom switch probability has been measured as a function of the pulse surface voltage for both n and p type doped silicon samples (see Fig. 11 page 17). For n type doped silicon, the switching probability has a maximum for surface voltages around -3.0 V as observed at room temperature [16]. Very surprisingly, we have found that the switching process is very unefficient for p type doped silicon. This is most probably related to the charging effects of surface states of silicon samples which are known to depend on the type of dopant in silicon [7]. We emphasize that such charging effects may have important implications in the charge transport along atomic lines although they have been neglected in the calculations by Doumergue et al. [13]. Preliminary experiments of charge transport along silicon dangling bond lines have been performed as illus-

trated in **Fig. 12**. After fabricating a 3 dangling bond line, the switching of a dangling bond at one end has been activated by injecting positive charges (-2.5 V surface voltage pulse) at the other end with the STM tip. Although much further measurements as a function of the atomic line length and for different types of atomic lines are needed, these preliminary results demonstrate the feasibility of measuring the charge transport efficiency along well defined atomic lines on the hydrogenated silicon surface.

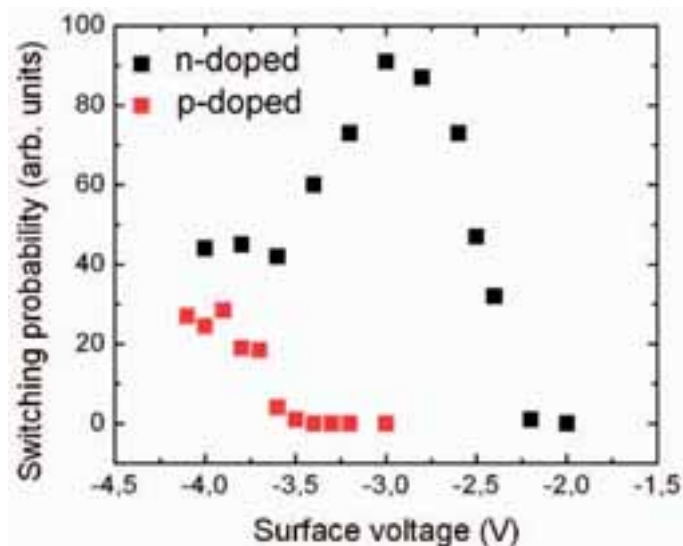


Figure 11: Switching probability (arbitrary units) of the atom switch as a function of the pulse surface voltage for *n* and *p* type doped Si(100).

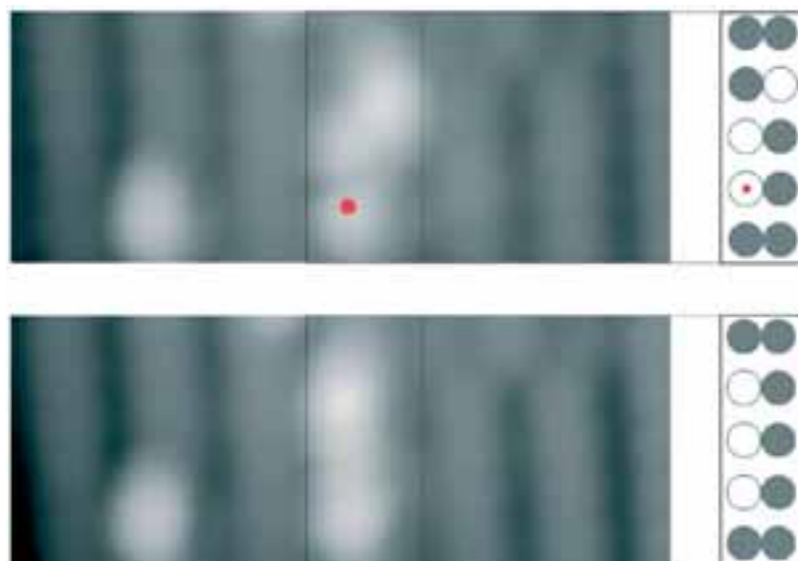


Figure 12: Low temperature STM topographies ($5 \times 1.9 \text{ nm}^2$, $V_S = -1.7 \text{ V}$, $I = 69 \text{ pA}$) showing the activation of the atom switch through charge transport along the dangling bond line. The top STM topography shows the initial system. Then, a pulse voltage (-2.5V) is applied with the STM tip at the red dot position. The bottom STM topography shows that the atom at the other end of the dangling bond line has been switched.

4. Conclusions

The biphenyl molecule adsorbed on the Si(100) is an interesting prototype of bistable molecule. Low temperature STM experiments have enabled us to investigate with a picometer scale precision the dynamics of the molecule after electronic excitation inside the molecule. We have shown that removing a single hydrogen atom in the vic-

nity of the molecule markedly modifies the dynamics of the molecule which becomes a multistable molecule. The type of dopant in the silicon has been shown also to strongly influence the molecular dynamics through electrostatic interactions between charges distributed inside the molecule and charged surface states. These results are anticipated to have important applications in molecular electronics for high precision control of molecular conformation.

With the aim to further electronically isolate the molecule from the substrate, we have investigated the fabrication and the properties of two kinds of insulating layers on Si(100), namely calcium fluoride and hydrogen. Thin layers of calcium fluoride offers interesting properties, i.e. a surface band gap of about 4 eV and 1D structuration, which can be exploited for positioning and electrically connecting molecules. The hydrogenated Si(100) surface offers a surface band gap of only 2 eV. However, hydrogen atoms can be manipulated one by one with the STM tip. By this way, charge transport along atomic lines on the surface can be tested.

So far, low temperature molecular electronics experiments have been limited to relatively narrow band gap semiconductors such as silicon (band gap 1.1 eV). In the future, it might be possible to extend such studies to wide band gap semiconductors such as silicon carbide (band gap 3.0 eV) or diamond (band gap 5.5 eV). This would open exciting perspectives to electrically contact single molecules and to further address them optically.

References

- [1] J. Repp, G. Meyer, S. M. Stojkovic, A. Gourdon and C. Joachim, **Phys. Rev. Lett.** **94**, 026803 (2005).
- [2] L. Gross, K.H. Rieder, F. Moresco, S.M. Stojkovic, A. Gourdon and C. Joachim, **Nature Materials** **4**, 892 (2005).
- [3] M. Lastapis, M. Martin, D. Riedel, L. Hellner, G. Comtet and G. Dujardin, **Science** **308**, 1000 (2005).
- [4] G. Dujardin, A.J. Mayne and F. Rose, **Phys. Rev. Lett.** **89**, 36802 (2002).
- [5] R.A. Wolkow, G.P. Lopinski, D.J. Moffart, **Surf. Sci.** **416**, 1107 (1998).
- [6] K. Hata, S. Yoshida, H. Shigekawa, **Phys. Rev. Lett.** **89**, 286104 (2002).
- [7] L. Liu, J. Yu and J.W. Lyding, **Mat. Res. Soc. Symp. Proc.** **705**, Y6.6.1 (2002).
- [8] M. Martin, M. Lastapis, D. Riedel, G. Dujardin, M. amatkulov, L. Stauffer and P. Sonnet, **Phys. Rev. Lett.** **97**, 216103 (2006).
- [9] X. H. Qiu, G. V. Nazin and W. Ho, **Science** **299**, 542 (2003).
- [10] R.A. McKee, F.J. Walker and M.F. Chisholm, **Phys. Rev. Lett.** **81**, 14 (1998).
- [11] H. Rauscher et al. **Chem. Phys. Lett.** (2004).
- [12] H. L. Pasquali et al. **Phys. Rev.** **B72**, 045448 (2005).
- [13] P. Doumergue, L. Pizzagalli, C. Joachim, A. Altibelli and A. Baratoff, **Phys. Rev. B** **59**, 15910 (1999).
- [14] T. Hitosugi et al. **Phys. Rev. Lett.** **82**, 4034 (1999).
- [15] L. Soukiassian, A.J. Mayne, M. Carbone and G. Dujardin, **Phys. Rev. B** **68**, 035303 (2003).
- [16] U.J. Quaade, K. Stokbro, C. Thirstrup and F. Grey, **Surf. Sci.** **415**, L1037 (1998).

NANO Vacancies - <http://www.phantomsnet.net/Resources/jobs.php>

✚ **PhD Position (Leibniz Institute, Germany):** *"RT9: Imaging CNT: micro-MRI and NMR studies"*

✚ **PhD Position (Leibniz Institute, Germany):** *"RT8: Imaging ferromagnetic CNT: spatially resolved SQUID studies"*

The CARBIO partners apply a multidisciplinary approach to exploit the potential of multi-functional carbon nanotubes (CNT) for biomedical applications, in particular to act as magnetic nano-heaters, drug-carrier systems and sensors which allow a diagnostic and therapeutic usage on a cellular level.

Please have a look at our website: <http://www.carbio.eu/carbio>

Contact Person: Bennie ten Haken (Leibniz Institute, Germany) / B.tenHaken@tnw.utwente.nl

✚ **PhD Positions (CIC nanoGUNE Consolider, Spain):** *"Nanoelectronics and Nanophotonics"*

The Nanoscience Cooperative Research Center CIC nanoGUNE Consolider invites applications for two positions as PhD Students.

Contact Person: Director (CIC nanoGUNE Consolider, Spain) / director@nanogune.eu

✚ **PhD Positions (Centro de investigación Nanociencia y Nanotecnología (CIN2) (CSIC: ICN), Spain):** *"2 PhD positions in Thin Film Nanostructures for a new generation"*

Future generations of portable devices (laptop computers, palm PC, mobilePhones, etc...) require higher power consumption, lighter weight, and longer lasting battery refill. Solid Oxide Fuel cell technology devices have two distinct advantages over present Li batteries: higher energy density per weight unit and rapid refuelling.

Applicants (Postgraduate students with a Physics, Chemistry or Materials Engineering degree) are requested to send their CV and the contact details of two referees by email to santiso@icmab.es (Ref.: PhD Nanoionics)

✚ **PhD Position (Institute of Optics-CSIC, Spain):** *"Theoretical aspects of optical manipulation and spatio-temporal control of light on the nanometer and femtosecond scales"*

Our group has recently contributed to demonstrate the control of light on the subwavelength domain by means of ultra-short laser pulses that are tailored in time at will and that interact with strategically patterned nanostructures. The successful candidate will apply and extend our theoretical methods to study the evolution of light in complex nanostructures in order to better understand the details of the noted control and to explore new schemes of light manipulation.

Contact Person: Javier García de Abajo (Institute of Optics-CSIC, Spain) / jga@io.cfmac.csic.es

✚ **PostDoctoral Positions (Institute of Optics-CSIC, Spain):** *"In nanophotonics to study theoretical aspects of optical manipulation and spatio-temporal control of light on the nanometer and femtosecond scales"*

Two postdoctoral positions in nanophotonics are open at the Spanish Scientific Research Council (CSIC) in Madrid (Spain) to study theoretical aspects of optical manipulation and spatio-temporal control of light on the nanometer and femtosecond scales.

Contact Person: Javier García de Abajo (Institute of Optics-CSIC, Spain) / jga@io.cfmac.csic.es

✚ **PhD Position (ICMM-CSIC, Spain):** *"Laser Optical Tweezers experiments to measure Protein-DNA and/or protein-protein interactions"*

Graduate student of Physics with a good background in Optics and with a strong motivation in Molecular Biology. The successful candidate will have to collaborate with biochemists.

Contact Person: Arturo Baro (ICMM-CSIC, Spain) / a.baro@icmm.csic.es

NANO Vacancies - <http://www.phantomsnet.net/Resources/jobs.php>

✚ **Scientist Positions (IMDEA-Materials (Madrid Institute for Advanced Studies of Materials), Spain):** "IMDEA-materials is looking for scientists at the senior and junior level to develop its first research lines in close collaboration with universities, research centers and companies in the region of Madrid"

IMDEA-materials is committed to excellence in research and to foster technology transfer to the industrial sector in a truly international environment.

Interested candidates should submit their Curriculum Vitae, a one-page statement of the research objectives as well as complete contact information for two references through the web page of the institute (<http://www.imdea.org/internationalcall>) or directly by e-mail to the Director of the Institute, Prof. Javier Llorca, javier.llorca@imdea.org

✚ **PostDoctoral Position (Universidad de Oviedo, Spain):** "Nanoscience Project in Nanomagnetism"

Applications are invited for a Post-doctoral position in the Laboratory of Thin Films to work on a coordinated project (reference NAN2004-09087), that involves three academic teams working on experimental and theoretical aspects in the area of Nanoscience in patterned magnetic films.

Contact Person: José I. Martín (Universidad de Oviedo, Spain) / jmartin@condmat1.ciencias.uniovi.es

✚ **PhD Position (ICMSE-CSIC, Spain):** "Post Doctoral fellow NOE-EXCELL Project"

Design and commissioning of magnetron sputtering kit. Experimental work with multifunctional coatings: preparation and characterisation. Supporting measures to report elaboration within the EXCELL network.

Contact Person: Asuncion Fernandez / Miguel Angel Muñoz (ICMSE-CSIC, Spain) / asuncion@icmse.csic.es / miguel.angel@icmse.csic.es

✚ **Silicon Photonics Engineer (Das Photonics, Spain)**

We are looking for a professional with expertise and eagerness to learn in the field of Silicon Photonics, especially from a design point of view. Project management experience and abilities are a plus.

Send resume to David Zorrilla - dzorrilla@dasphotonics.com - Reference: SiPh

✚ **PhD Position (CEA, France):** "Theory of Thermal and Thermoelectric Transport"

We are looking for talented individuals whose expertise and interests can contribute to the theoretical and computational investigation of thermal, electronic, and thermoelectric transport through nanostructured materials and/or nanoscale devices. The theoretical research will be conducted in parallel with experimental work carried out at LITEN and several other laboratories in the U.S. and France.

Interested candidates should send their resume, publication list, and contact information for at least three references, electronically to Dr. Natalio Mingo, e-mail: natalio.mingo@cea.fr . Applications will be accepted until position is filled.

✚ **PhD Position (IEMN-CNRS, France):** "STM studies of organic monolayers for opto-electronic molecular memories"

Experimental work of our team relates to the electron transport properties of organic nanostructures (self-assembled monolayers, organic nano and micro-crystals, supra-molecular assemblies ...) and their applications in molecular-scale electronics and organic electronics. See: http://www.iemn.univ-lille1.fr/sites_perso/vuillaume/MolElec.html

The applicant should send his/her CV, summary of previous work and recommendation letters by e-mail or mail to: S. Lenfant, e-mail: stephane.lenfant@iemn.univ-lille1.fr or D. Vuillaume, e-mail: dominique.vuillaume@iemn.univ-lille1.fr

NANO Conferences - <http://www.phantomsnet.net/Resources/cc.php>

(August 2007)

✚ **CFN Summer school on Nanobiology.**
August 28-31, 2007. Bad Herrenalde (Germany)
<http://www.cfn.uni-karlsruhe.de>
NanoBiotechnology

✚ **CFN Summer school on Nanoelectronics.**
August 20-23, 2007. Bad Herrenalde (Germany)
<http://www.cfn.uni-karlsruhe.de/>
Nanoelectronics

(September 2007)

✚ **The Second International Conference on One-dimensional Nanomaterials.**
September 26-29, 2007. Malmö (Sweden)
<http://www.pronano.se/~icon>
NanoMaterials, Nanotechnologies

✚ **33rd International Conference on Micro- and Nano-Engineering (MNE2007).**
September 23-26, 2007. Copenhagen (Denmark)
<http://www.mne07.org/>
NEMS & MEMS, NanoFabrication, NanoImprint

✚ **NanoForum2007.**
September 18-19, 2007. Politecnico of Milan (Italy)
<http://www.nanoforum.it/english/english.htm>
Nanotechnology Business, Nanotechnologies

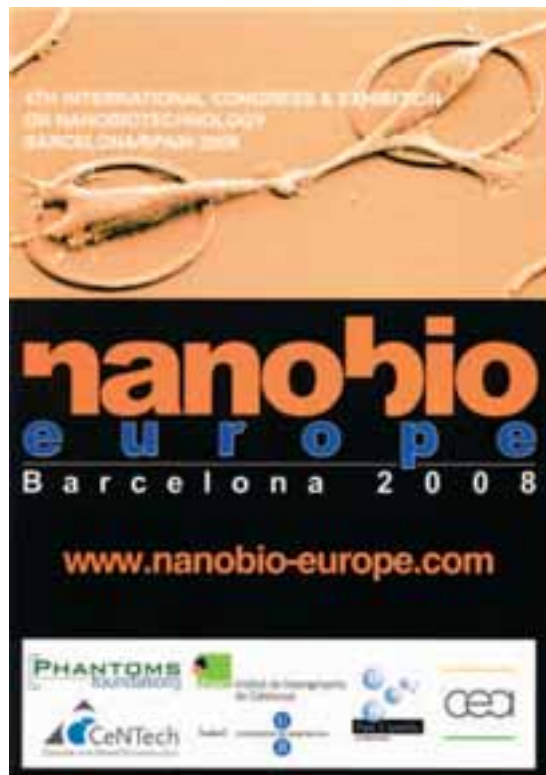
✚ **International Conference Chirality at the Nanoscale.**
September 17-21, 2007. Sitges - Barcelona (Spain)
<http://chiralitynanoscale2007.congress-uex.com>
NanoChemistry

✚ **10th International Conference on Non-Contact Atomic Force Microscopy.**
September 16-20, 2007. Antalya (Turkey)
<http://nano.bilkent.edu.tr/~ncafm07/>
NanoProbes

✚ **7th International Workshop on Future Information Processing Technologies.**
September 04-07, 2007. Dresden (Germany)
<http://www.iwfip.gwtonline.de/>
Nanoelectronics

✚ **Trends in Nanotechnology (TNT2007).**
September 03-07, 2007. San Sebastian (Spain)
<http://www.tnt2007.org/>
Nanoelectronics, NanoMaterials, NanoBiotechnology

✚ **9th European Conference on Surface Crystallography and Dynamics (ECSCD-9).**
September 02-05, 2007. Vienna (Austria)
<http://www.iap.tuwien.ac.at/www/ecscd9/index.html>
Theory & Modeling, Nanotechnologies



NANO News - <http://www.phantomsnet.net/Resources/news.php>

☒ **PICMOS demonstrates first optical interconnect layer on silicon (July 04, 2007)**

<http://www.opticsinfobase.org/abstract.cfm?URI=oe-15-11-6744>

A compact, electrically driven light source integrated on silicon is a key component for large-scale integration of electronic and photonic integrated circuits.

Keywords: Nanophotonics & Nano-Optoelectronics

☒ **Nanotechnology fabrication depends on sophisticated simulation tools (July 03, 2007)**

<http://www.nanowerk.com/spotlight/spotid=2163.php>

Increasing research in the field of nanoelectronics also requires the rise of a new generation of supporting fields, such as modeling and simulation tools.

Keywords: Nanofabrication / Nanoelectronics / Theory & Modeling

☒ **Carbon nanotubes endure heavy wear and tear (July 02, 2007)**

<http://www.physorg.com/news102610525.html>

The ability of carbon nanotubes to withstand repeated stress yet retain their structural and mechanical integrity is similar to the behavior of soft tissue, according to a new study from Rensselaer Polytechnic Institute.

Keywords: Nanotubes

☒ **Asylum Research Announces Collaboration with the Institute of Microelectronics of Madrid (IMM) on Advanced AFM Cantilever Dynamics (July 02, 2007)**

http://www.nanotech-now.com/news.cgi?story_id=23608

Asylum Research has announced its collaboration with Prof. Ricardo Garcia's lab in the Institute of Microelectronics of Madrid (CSIC) to further develop new techniques in the field of AFM cantilever dynamics, focusing on higher harmonic and multiple frequency measurement modes.

Keywords: Nanoprobes / SPM

☒ **Bright future for nanowire light source (June 28, 2007)**

<http://www.physorg.com/news102256632.html>

Among the many potential applications of the nano-sized light source, once the technology is refined, are single cell endoscopy and other forms of subwavelength bio-imaging, integrated circuitry for nanophotonic technology, and new advanced methods of cyber cryptography.

Keywords: Nanofabrication / Nanophotonics & Nano-Optoelectronics / Nanobiotechnology

☒ **Transistors based on carbon nanotubes get faster and faster (June 27, 2007)**

<http://www2.cnrs.fr/en/923.htm>

Researchers at the Institute of Electronics, Microelectronics and Nanotechnologie and the Department of Solid-state Physics at the French Atomic Energy Agency (CEA), have succeeded in making transistors from carbon nanotubes on a silicon substrate.

Keywords: Nanotubes / Nanoelectronics

☒ **German nano spending outstrips that of other Member States (June 22, 2007)**

<http://cordis.europa.eu/search/index.cfm?fuseaction=news.simplifiedocumentLucene&RCN=27904>

Germany is by far investing more in nanotechnology than other European country. Worldwide, Japan's spending on nano is set to overtake that of the US, and the EU as a bloc comes third after these two countries.

Keywords: Scientific Policy

☒ **Catching Waves: Measuring Self-Assembly in Action (June 21, 2007)**

http://www.nist.gov/public_affairs/techbeat/tb2007_0621.htm#waves

These results should be important to understanding self-propagating chemical reactions and ordering and self-assembly phenomena in situations involving confinement, such as thin films and the porous internal geometries of many materials, such as rocks and cement.

Keywords: Self-Assembly

☒ **Electron beam 'carves' the world's smallest devices (June 18, 2007)**

<http://www.physorg.com/news101406081.html>

Physicists at the University of Pennsylvania are using a new technique to craft some of the tiniest metal nanostructures ever created, none larger than 10 nanometers.

Keywords: Nanofabrication

Quick & Clean: Advances in High Resolution Stencil Lithography

Juergen Brugger, Veronica Savu, Katrin Sidler, Marc van den Boogaart, Oscar Vazquez Mena and Guillermo Villanueva
Microsystems Laboratory, Swiss Federal Institute of Technology, Ecole Polytechnique Federale de Lausanne (EPFL), 1015 Lausanne, Switzerland

Contact: nanostencil@epfl.ch; Web pages: <http://lmis1.epfl.ch>, <http://lmis1.epfl.ch/nanostencil>

Introduction

Lithography is the main process step for the fabrication of integrated micro- and nano-electro-mechanical systems (MEMS/NEMS). In recent years, due to the continuous miniaturization and integration of devices, lithography techniques have been pushed well into the sub-100-nm scale for industrial applications. For meeting the specifications of micrometer and nanometer scale devices, photolithographic techniques associated with pattern transfer methods rely on well defined and tight process parameters. Surface patterning using lithography is a subtractive method. This means that the material is first deposited everywhere and then reduced to the desired shape by lithography and etching methods. This procedure involves a series of processing steps and associated sub-steps such as: thin film deposition, photo-resist spinning, exposure, development, etching, and finally resist removal. All these steps need to be performed for each layer in the process. In the case of materials that are difficult or impossible to etch, a so-called 'lift-off' process is used. Here, first a photoresist is deposited and structured by lithography, and then the thin film is deposited over the substrate which is partially covered with resist. Finally, the resist layer is dissolved whereby unwanted material is lifted off the surface.

Standard lithography with the associated process steps such as thin film deposition, photo-resist spinning, exposure, development, etching, and finally resist removal find technical limitations in the case of surfaces that are (bio)chemically functionalized, mechanically fragile or three dimensional, or when there is a poor etch selectivity between the aimed surface pattern and the substrate. Another, rather economical than technical, hurdle is the high cost of nanolithography for niche applications outside the mainstream semiconductor field. These technological and economic barriers prevent efficient progress in research and development in many application fields of micro and nanosystems.

In the frame of the EU funded Integrated Project "NaPa" (Contract No NMP4-CT-2003-500120) a series of alternative emerging nanopatterning methods is being developed to overcome this bottleneck. They are complementary to standard lithography processes and include e.g. scanning probe methods, soft-lithography or microcontact printing (μ CP), nanoimprint lithography (NIL), MEMS-based nanopatterning using probes and stencils, as well as self-assembly. They allow for versatile, flexible, and multi-material patterning with high throughput and are promising candidates for cost feasible nanomanufacturing. The new emerging patterning methods have the capability to cover

multiple length-scales from molecular scale to centimeters. Consequently they are considered to be good candidates for bridging between the classical top-down miniaturization methods with central control by lithographic engineering, and the bottom-up self-organization strategies with distributed control by nature driven self-assembly.

μ CP, NIL and stencil lithography (SL) are replication methods, which means that a mother structure is copied in multiple daughter (or son?) structures. The three methods are complementary to each other and form part of a versatile tool-box for cost-efficient, flexible, top-down nanofabrication. Both μ CP and NIL rely on a physical contact between a master surface (stamp) and the surface to be patterned. This is in contrast to the local deposition via nanostencils, which is a potentially a contact-less method thus offering promising alternatives to define micro and nanoscale surface structures without actually touching the substrate. This obviously makes the method extremely interesting for patterning fragile surfaces. In addition, stencil lithography is done in vacuum, without exposing the substrate and deposited material to atmosphere, which enables the engineering of new nanodevices with superior material and interface. This paper gives an overview of the basic principle of stencil fabrication and its application as a lithography tool, along with some typical recent results.

What is Stencil Lithography?

Stencil Lithography (SL) is a patterning technique which uses a shadow mask (i.e. stencil membrane with apertures) to block part of a directed material flux [1]. **Fig. 1-page 23** shows a schematic representation of the 3 steps involved in the SL process. First, the stencil is aligned (if needed, e.g. [2]) and fixed on to a substrate. Second, the stencil/substrate combination is placed in a material flux (e.g. generated by a physical vapor deposition process) and a controlled amount of material is deposited on and through the stencil. The third step consists of the stencil being removed, leaving the apertures within the stencil replicated on the target substrate. The stencil can be reused for subsequent stencil lithographic processes [3].

Fabrication of micro- and nano-stencils

The fabrication process for stencils and/or stencil membranes contains several steps. In particular, stencils using thin-film solid-state membranes are fabricated by means of standard MEMS processing. **Fig. 2 page 23** shows a schematic illustration of the fabrication of thin-film stencils. The stencil fabrication scheme as shown in **Fig. 2** can be applied to roughly any type of thin-film stencils composed of Si and a membrane material (SiN, SiO₂, etc.). The process starts by the deposition of a membrane material on a 100 mm Si wafer (**Fig. 2a and 2b**). The choice of the membrane material has a direct influence on the available aperture definition technologies, membrane release methods and application fields. The higher selectivity of SiN than that of Si during the release of the membrane in KOH makes SiN the preferred membrane material. Furthermore, SiN can easily be tuned to a low-stress state

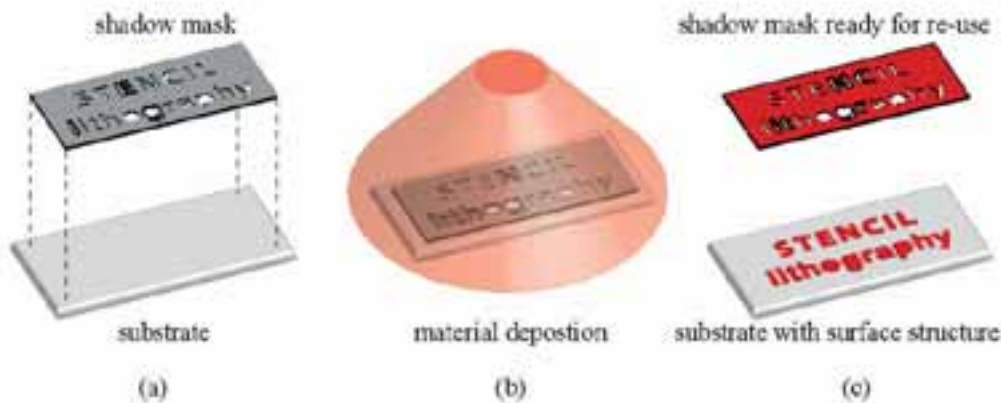


Figure 1: Schematic representation of static stencil lithography. (a): a stencil is brought in contact or proximity to a substrate, (b): the stencil/substrate combination is placed in a deposition chamber and a controlled amount of material is deposited through the stencil onto the substrate and, (c): the stencil is removed from the substrate. The apertures in the stencil are successfully transferred onto the substrate and the stencil can be reused for a subsequent process step. Image from [51, 52].

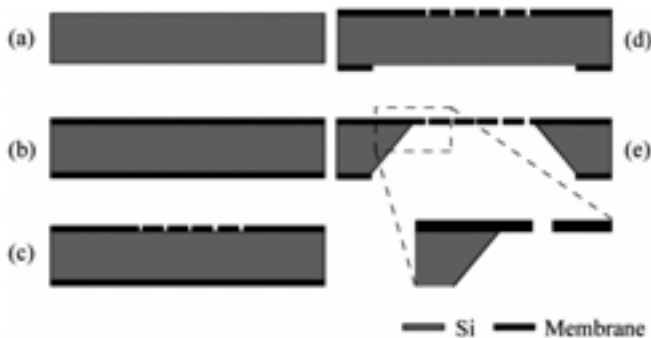


Figure 2: A simplified schematic for the fabrication of thin-film stencil membranes. (a): the process starts with a (100 mm) Si wafer; (b): deposition of a membrane material (e.g. SiN), (c): membrane aperture definition, (d): membrane etch mask definition in the back-side membrane material and (e): membrane release from bulk by etching through the wafer. Image from: [51, 52].

(Silicon rich SiN), which allows the definition of larger membranes and a better yield. Then, the designed membrane apertures are transferred into the previously deposited membrane layer (Fig. 2c), followed by the definition of the membrane size in the backside SiN (Fig. 2d). The realization of micro/nano apertures in thin-film stencil membranes can be achieved using a large range of available processes and techniques. These techniques involve either a lithographic process step followed by the transfer of the defined patterns into the membrane, or a direct patterning technique where the membrane apertures are directly opened (e.g. Focused Ion Beam [4-9]). Ultra-Violet (UV) photolithography remains (for now) the preferred patterning technique for micron scale apertures. However, the use of Deep-Ultra-Violet (DUV, e.g. [10]) or other new and complementary lithography techniques such as Laser Interference Lithography (LIL, e.g. [11]), Nano Imprint Lithography (NIL), Electron-Beam Lithography (EBL, e.g. [12-16]) are constantly under development and increasingly being used.

Releasing the membrane from the bulk Si is, after aperture definition, one of the more critical fabrication steps (Fig. 2e). The membrane material, along with the aperture size and shape, has a direct influence on the success of the release technique. SiN has a higher selectivity than Si to KOH or TMAH, making these techniques the preferred ones for releasing SiN membranes from bulk Si. The downsides of wet chemical release are the increased probabilities for membrane rupture and stiction. Stiction of thin membrane bodies can be avoided by a dry etch membrane release process. An additional important advantage of a dry-etch release over a wet-etch release is the possibility to increase the active surface area of the stencil, i.e. to have a higher density of membranes within a stencil.

Reinforced membranes for improved pattern transfer

Reinforced membranes for improved pattern transfer

Thin, planar stencil membranes deform under the influence of deposited material stress. The difference in thermal expansion coefficients and the lattice spacing mismatch are thought to be the dominant sources of deposition-induced stress, causing a substantial deformation of the micromachined bi-layered structures [17-19].

Fig. 3 page 24 shows the effect of membrane deformability on the deposited surface structures in two situations. The first image (Fig. 3a) shows the ideal situation of a stencil deposition process in which the stencil membrane does not deform. In this situation, the dimension and shape of the deposited surface pattern can be described by a simple model based on geometrical considerations (e.g. [8, 20-31]). The other two images (Fig. 3b, 3c) show the deposition process using a non-supported stencil in which the membrane is deformed and the initial gap is increased during deposition - for instance, due to high-stress material deposition or unstable membrane aperture configurations. The consequent changes in membrane aperture geometry (Δx in Fig. 3c) and the increased gap between stencil membrane and substrate (Δz in Fig. 3c) result in pattern distortion and blurring (i.e. reduced edge sharpness and limited spatial resolution) of the deposited surface structures.

New stabilization schemes, which increase the moment of inertia of the active membrane area and are based on MEMS processes, have been developed:

(1) An in-situ scheme which increases the moment of inertia of thin stencil membranes based on the introduction of corrugations within the membrane (Fig. 4b page 24 and [32]). These corrugated SiN membranes are fabricated by adding one process step to the standard stencil fabrication process as previously discussed. This simple process resulted in considerably more, stable membranes,

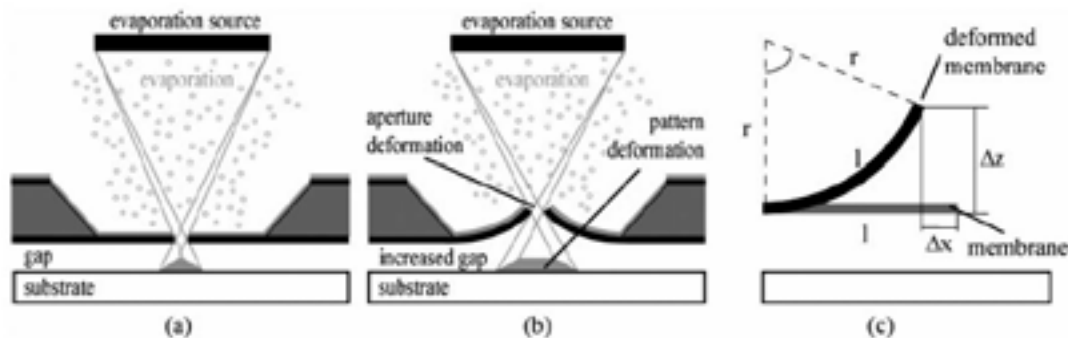


Figure 3: Schematic representation of a stencil membrane in close proximity to a substrate during evaporation. (a): ideal stencil deposition (non-deformed membrane). The membrane does not deform, thus not contributing to pattern deformation; (b): stencil deposition using a non-supported stencil membrane (deformed membrane). The deformed membrane has both an increased gap (Δz) and an aperture deformation (Δx), resulting in uncontrollable pattern deformation; (c): deformed membrane showing both an increased gap (Δz) and an aperture deformation (Δx). Image from: [51, 52].

yielding well-defined surface patterns. However, the ratio (height: width) of the corrugations cannot be varied unlimitedly due to the thin corrugated wall thickness (determined by the membrane thickness). This limits the total increase in membrane stiffness that can be achieved with corrugations [32,33]. (2) An additive scheme which increases the moment of inertia of thin stencil membranes by the addition of a second, complementary layer (e.g. Si) on top of the membrane (Fig. 4a and [34]). A mono-crystalline Si-support is formed by bulk Si, allowing for relatively thick and therefore stable membranes. The fabrication of Si-supported membranes however requires more elaborate processing [35] compared to the corrugated stencil fabrication.

Applications of SL

As mentioned earlier, stencil lithography is complementary to other lithography steps (UV, DUV, EBL, but also μ CP and NIL) in the sense that material is locally deposited in a single step on the surface exactly where it is needed (Fig. 5 page 25); no further processing is necessary. Let us have a look at a few examples where this uniqueness can be exploited. In the following paragraphs we present some typical applications where SL can enable new devices or reduce manufacturing time and costs.

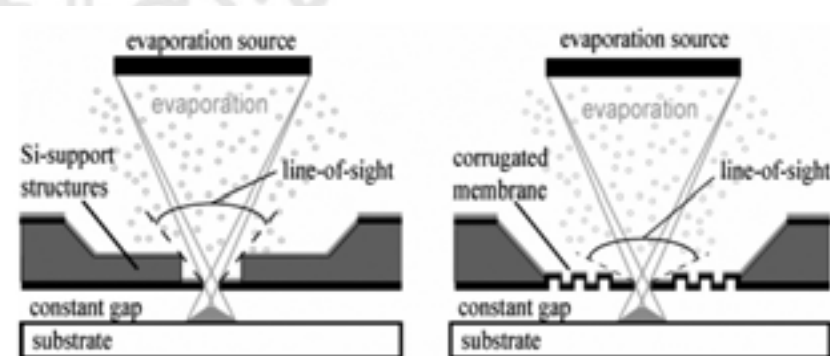


Figure 4: Mechanically improved stabilized membranes. (a): Si-supported stencil lithography and (b): corrugated stencil lithography. The membrane is locally supported on the side facing the material flux and does not affect the "line-of-sight", allowing the smallest possible gap. Image from: [51, 52].

Stenciling nanowires

An important application of stencil lithography is the fabrication of nanowires. One of the most interesting characteristics of such structures is their high surface-to-volume ratio, making any nanowire interface modifications or events (e.g. electrical gating, photon exchange) be relevant to their properties [36, 37]. Nanowires have proven their utility for electronic components such as transistors [38],

logic gates [39], optoelectronic devices [40] and biological [41] and chemical sensors [42].

Stencil lithography offers a top-bottom approach for the fabrication of precisely located nanowires at low cost and with simple processing. Al and Au 1-D structures have been fabricated reaching dimensions on the order of 100 nm [3, 43]. Different materials, such as organic molecules or oxides, can also be patterned in similar geometries. One major advantage of SL is the fabrication of nanowires relying only on simple PVD methods, without any resist-based process. The stencils can also be reused, lowering thus the fabrication costs.

Pulsed Laser Deposition – a soft landing method for functional material

One of the challenges in molecular electronics is the fabrication of micro-electrodes on self-assembled monolayers (SAMs). The deposition of a top electrode on the SAM can damage the SAM (with a characteristic thickness of a couple of nm) through the impact of the highly-energetic incoming atoms, and the electrodes can become shorted due to the diffusion of the deposited material through the SAM.

Speets et al. [44] used pulsed laser deposition (PLD) through nano- and microstencils to fabricate noble-metal structures on top of octadecanethiol (ODT) SAMs, on Au substrates. They employed two methods. First, they deposited 3-4 nm of different metals (Pd, Cu, Pt), with sizes from 500 nm to few hundred micrometers. Fig. 6a page 25 shows the SEM image of part of the SiN nanostencil, with 500 nm diameter pores. The metal islands obtained by PLD through this stencil are shown in Fig. 6b-d page 25. In the second experiment, they grew Cu structures based on noble-metal clusters used as catalysts for selective electroless deposition (ELD). These methods were successful in fabricating electrode without damaging the SAMs or shorting to the substrate.

Miniaturization of electronics devices promp-

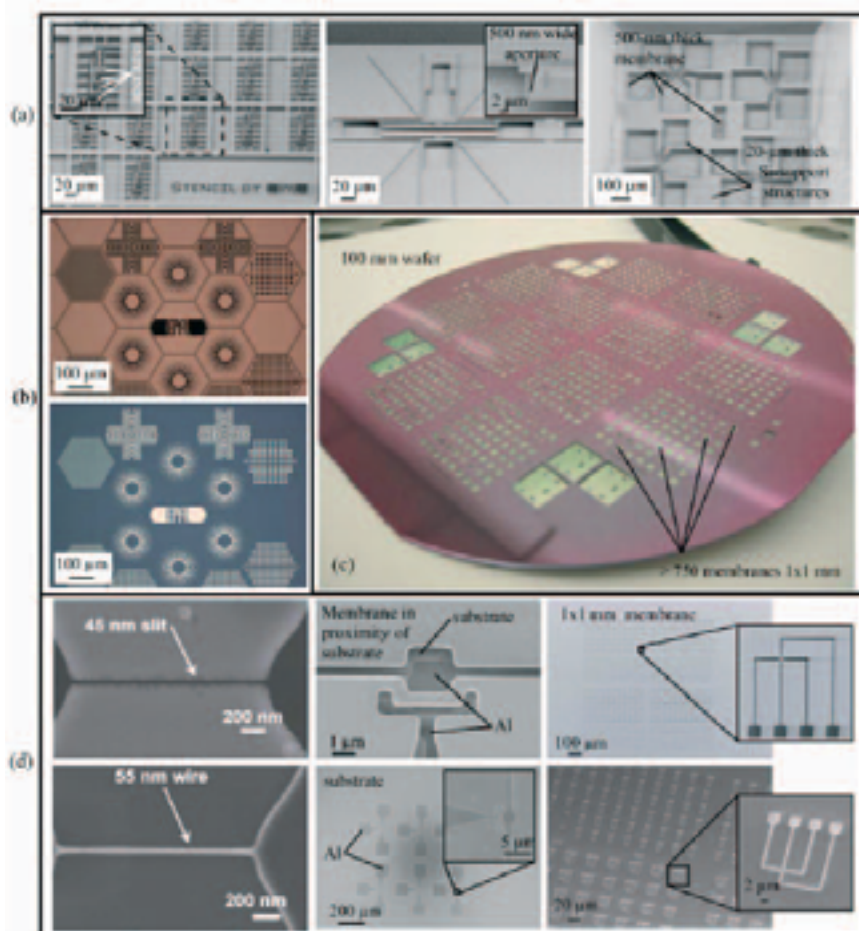


Figure 5: Collection of images. **(a)** Three SEM images of reinforced 500-nm-thick SiN membranes; **(b)**: Optical images of micro stencil membrane (top) and the resulting surface patterns (bottom); **(c)**: An optical image of a full wafer stencil (100 mm) containing numerous membranes (1x1 mm²) each containing multiple micro and nanoapertures; and **(d)**: Images show membrane and resulting surface structures.

ted research towards the integration of complex functional materials in the standard silicon-based technology, including the relationship between the functional properties of ferroelectric materials and their structure and size.

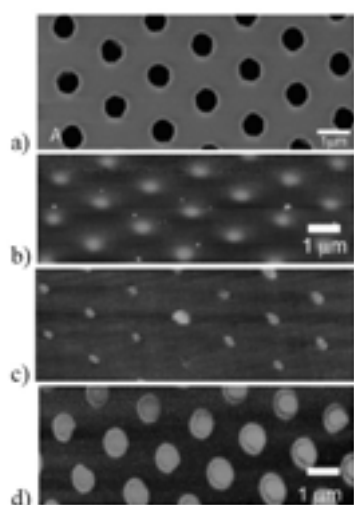


Figure 6: Noble metal patterns created by PLD with stencil lithography on self assembled monolayers (SAMs) **(a)** Scanning electron microscope (SEM) image of a SiN nanostencil with 500 nm diameter pore; AFM images of structures patterned with the nanostencil on the SAM, made of **(b)** Pd, **(c)** Cu, and **(d)** Pt. Image from [44].

The resist-based patterning techniques are known to induce surface damages and contamination, which become relevant when the interface engineering is key to the functioning of the device, and when submicron elements are the goal.

PLD through a stencil was used [45] for patterning ordered arrays of nanostructures barium titanate (BaTiO₃) on different substrates. After a postdeposition annealing treatment, x-ray diffraction pattern showed a nanocrystalline BaTiO₃ structure close to the perovskite cubic phase, with grains 30-35 nm in size. Their local ferroelectric properties were investigated using piezoresponse force microscopy.

Integrated NEMS on CMOS – alignment accuracy and dimension control

In 2006, Arcamone et al. [2] succeeded in fabricating in parallel multiple (~2000) silicon nanomechanical resonators at the 200 nm scale, monolithically integrated into CMOS circuits. The strategy for the resonator fabrication was based on using existing CMOS layers as structural layer (polysilicon) and sacrificial layer (field oxide). After the fabrication of the CMOS cir-

cuits, an on-chip area dedicated to the integration of the nanodevices is patterned by evaporation of 80 nm Al through nanostencils (Fig. 7).

The main challenges were to achieve a 1 μm accurate alignment at wafer scale and to removal the unwanted but inherent Al blurring caused by the gap between the sten-

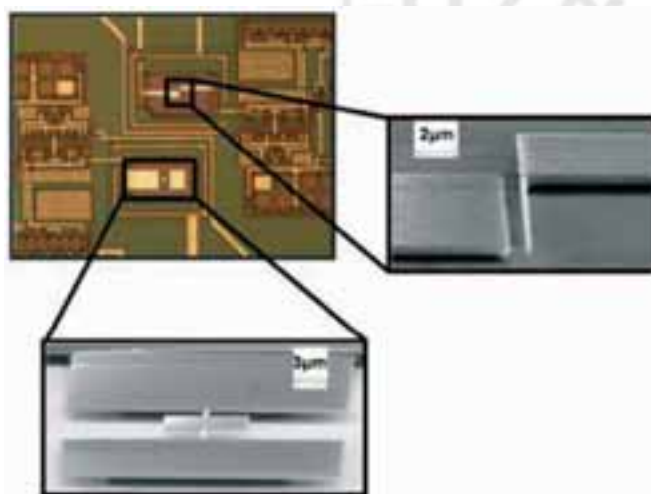


Figure 7: Different types of polysilicon resonators patterned by stencil lithography and etching, monolithically integrated with CMOS circuits. Image from [2].

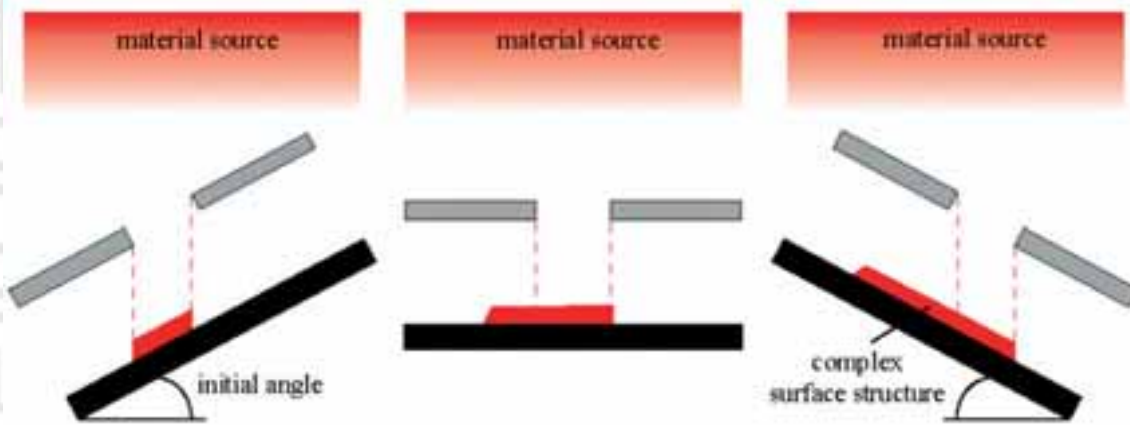


Figure 8: Angular Dynamic Stencil deposition. The shadow mask and the substrate are tilted with respect to the source, allowing the formation of complex structures. Image from [51, 52].

cil and the integration area. The blurring was successfully removed by a simple corrective dry etching [2].

Flexible / organic materials – bright & flexible future for MEMS/NEMS

During the last years, flexible electronics received increasing attention, especially for mobile applications such as display technologies. In particular, polymer substrates and organic semiconductors are of great interest for large arrays of thin film transistors [46]. Polymer materials enable devices to be flexible and to better withstand stress and strain under mechanical load. Patterning methods for metals on polymers are limited by the substrate's upper working temperature and its chemical incompatibility with solvents. Organic semiconductors have an electrical performance lower than amorphous Si, but many of them can be processed at lower temperatures, using techniques such as in-vacuum evaporation [47]. Additionally, organic semiconductors can be deposited on a large variety of substrates. Stencil lithography, being a resistless technique, is therefore the ideal candidate for patterning organic semiconductors and metals on polymer substrates.

Flexible pentacene field-effect transistors with polyimide gate dielectric layers on plastic films have been realized

[48]. Vacuum evaporation through a shadow mask was used to structure Cr/Au gate electrodes, pentacene films, Au drain and Au source electrodes at the sub-mm scale. The achieved channel length and width of the transistor were 1 mm and 100 μm , respectively. Such a flexible transistor and in particular its channel dimension could be easily miniaturized using thin-film membrane stencil lithography.

Dynamic Stencil – as ultimate in-vacuum nanopatterning machine

So far, only applications where the shadow mask is fixed have been presented. However, if the shadow mask is moved during the stenciling process, an enormous range of applications is opened. For the moment, the use of this kind of movable shadow masks has already been demonstrated for the fabrication of several structures, e.g. mechanical switches [49], tunnel junctions [15], epilayer structures [50], nano-interdigitated wires [9], etc.

Dynamic Stencil has been demonstrated using two different kinds of setups. The first option explores the possibilities of changing the angle between the source and the substrate (see Fig. 8). By tilting the substrate and the stencil at the same time with respect to the source, the material can be deposited in different places or continuously, generating a path onto the substrate [15, 16]. The other option implies maintaining all three planes (source, substrate and stencil) parallel, while moving the stencil (see Fig. 9). This can be made either in a step-and-repeat process (deposition, movement and deposition again) [50] or in a continuous process, where the evaporation is performed during the movement [4, 9].

In the latter, differences on the deposited patterns on the substrate can be observed, depending on the speed of the movement and also on the number of times the aperture is passing by the same place, allowing the actual drawing of patterns onto the substrate.

Although very impressive results have been already shown using this Dynamic Stencil technique, there is still need for the development of an experimental setup for the implementation of a full wafer dynamic stencil. This way stencils

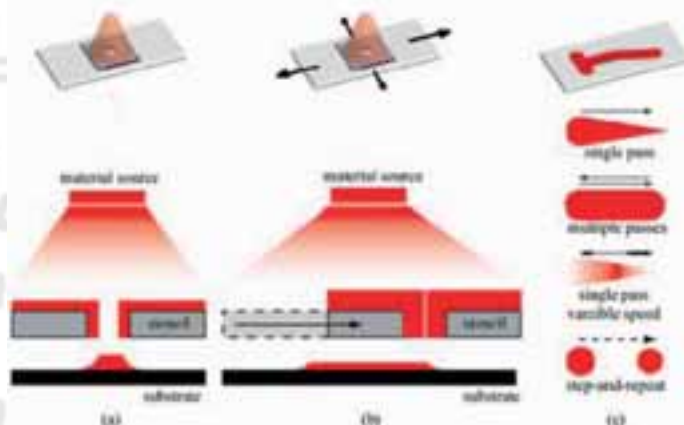


Figure 9: Schematics showing the working principle of the second option for dynamic stencil lithography. Starting from a standard deposition (a), the movement of the shadow mask (b) creates patterns onto the surface. Several possibilities are offered by this setup (c), including the step-and-repeat process, the variable thickness depending on the speed of the shadow mask and the variation of width. Image from [51, 52].

could be used for parallel patterning of full wafers for new applications.

Conclusions/outlook

This paper summarizes the progress and some recent highlights that were made in the field of high resolution shadow mask nanopatterning. Due to recent advances within our projects and in the research community, the technique is progressing steadily towards reliable sub-100 nm scale patterning on full-wafer scale. Earlier bottlenecks such as stencil membrane bending, pattern blurring, aperture clogging and alignment issues are overcome one by one by creative engineering solutions. Stencil lithography is inherently simple; all that is needed is a physical vapor deposition tool and stencils to create nanopatterns; no further step is necessary. This saves time, energy, material, and hence money. Ultimately it enables organizations without sophisticated infrastructure to gain access to nanotechnology. The remaining engineering challenges are being studied in detail. They concentrate currently on the optimization of gap control and overlay precision on full-wafer scale, as well as on the dynamic stencil tool allowing the movement of the stencil shadow mask during deposition in vacuum for the direct patterning of complex surface structures.

Acknowledgements

We are very pleased to acknowledge our colleagues from the EPFL Center of Micro and Nanotechnology for their contribution to the nanostencil work. Many thanks to our project partners in the MEMS-based subproject within the EU funded IP 'NAPA' with special thanks to the MESA+ Research Institute for Nanotechnology, University of Twente, The Netherlands, where the membrane nanostencil work started. Financial support for part of the work described here comes from an earlier EU FP5 project ATOMS, EU FP6 IP NAPA, the Swiss CTI Top-Nano 21 project "Melode", and from the Swiss Federal Institute of Technology, EPFL, Lausanne.

References

- [1] Brugger, J. and G. Kim, *Nanofabrication by shadow deposition through nanostencils, in Nanolithography and patterning techniques in microelectronics*. 2005, **Woodhead Publishing Limited**. p. 218-237.
- [2] Arcamone, J., et al. *Full wafer integration of NEMS on CMOS by nanostencil lithography in IEEE IEDM 2006 conference*. 2006. San Francisco (USA).
- [3] Vazquez, O., M.A.F. Van den Boogaart, and J. Brugger. *Towards Reliable 100-nanometer Scale Stencil Lithography on Full Wafer: Progress and Challenges. in Transducers'2007*. 2007.
- [4] Egger, S., et al., *Dynamic Shadow Mask Technique: A Universal Tool for Nanoscience*. **Nano Lett.**, 2005. 5(1): p. 15-20.
- [5] Lin, R., et al., *Micro-four-point-probe characterization of nanowires fabricated using the nanostencil technique*. **Nanotechnology**, 2004. 15(9): p. 1363.
- [6] Zahl, P., et al., *All-in-one static and dynamic nanostencil atomic force microscopy/scanning tunneling microscopy system*. **Review of Scientific Instruments**, 2005. 76(2): p. 023707.
- [7] Kim, G.M., M.A.F. van den Boogaart, and J. Brugger, *Fabrication and application of a full wafer size micro/nanostencil*

for multiple length-scale surface patterning. **Microelectronic Engineering**, 2003. In Press, Corrected Proof.

- [8] Köhler, J., et al., *Direct growth of nanostructures by deposition through an Si₃N₄ shadow mask*. **Physica E: Low-dimensional Systems and Nanostructures**, 1999. 4(3): p. 196-200.
- [9] Lüthi, R., et al., *Parallel nanodevices fabrication using a combination of shadow mask and scanning probe methods*. **App. Phys. Lett.**, 1999. 75(9): p. 1314-1316.
- [10] Van den Boogaart, M.A.F., et al., *DUV-MEMS stencils for high-throughput resistless patterning of mesoscopic structures*. **Journal of Vacuum Science and Technology B**, 2004. 22(6): p. 3174 - 3177.
- [11] Kuiper, S., et al., *Development and applications of very high flux microfiltration membranes*. **J. Mem. Sci.**, 1998. 150: p. 1-8.
- [12] Zhou, Y.X., et al., *Simple Fabrication of Molecular Circuits by Shadow Mask Evaporation*. **Nano Lett.**, 2003. 3(10): p. 1371-1374.
- [13] Champagne, A.R., et al., *Nanometer-scale scanning sensors fabricated using stencil lithography*. **Applied Physics Letters**, 2003. 82(7): p. 1111-1113.
- [14] Kamm, F.-M., et al., *Influence of Silicon on Insulator Wafer Stress Properties on Placement Accuracy of Stencil Masks*. **Jpn. J. Appl. Phys.**, 2002. 41(Part 1, No. 6B): p. 4146-4149.
- [15] Ono, K., et al., *A New Fabrication Method for Ultra Small Tunnel Junctions*. **Jpn. J. Appl. Phys.**, 1996. 35: p. 2369 - 2371.
- [16] Deshmukh, M.M., et al., *Nanofabrication using a stencil mask*. **Applied Physics Letters**, 1999. 75(11): p. 1631-1633.
- [17] Ohring, M., *The Material Science of Thin Films*. 1992: Academic Press.
- [18] Tarraf, A., et al., *Stress investigation of PECVD dielectric layers for advanced optical MEMS*. **Journal of Micromechanics and Microengineering**, 2004. 14(3): p. 317-323.
- [19] Chen, K.-S., X. Zhang, and S.-Y. Lin, *Intrinsic stress generation and relaxation of plasma-enhanced chemical vapor deposited oxide during deposition and subsequent thermal cycling*. **Thin Solid Films**, 2003. 434(1-2): p. 190-202.
- [20] Malzer, S., et al. *Properties and applications of the "epitaxial shadow mask molecular beam epitaxy technique". in The 15th North American conference on molecular beam epitaxy*. 1996: AVS.
- [21] Tian, P.F., P.E. Burrows, and S.R. Forrest, *Photolithographic patterning of vacuum-deposited organic light emitting devices*. **Applied Physics Letters**, 1997. 71(22): p. 3197-3199.
- [22] Suzuki, M., et al., *Silicon shadow mask MOVPE for in-plane thickness control of InGaAsP/InP structures*. **Journal of Crystal Growth**, 1997. 170(1-4): p. 661-664.
- [23] Ingle, F.W., *A shadow mask for sputtered films*. **Review of Scientific Instruments**, 1974. 45(11): p. 1460-1461.
- [24] T. Schallenberg, C.S., L. W. Molenkamp,, *Projective techniques for the growth of compound semiconductor nanostructures*. **physica status solidi (a)**, 2003. 195(1): p. 232-237.
- [25] Dolan, G.J., *Offset masks for lift-off photoprocessing*. **App. Phys. Lett.**, 1977. 31(5): p. 337 - 339.
- [26] Hammer, R., *Solving the "stencil" problem in vacuum deposition masks using rib-supported structures*. **Journal of Vacuum Science and Technology**, 1977. 14(05): p. 1208-1210.
- [27] Schallenberg, T., C. Schumacher, and W. Faschinger, *In situ structuring during MBE regrowth with shadow masks*. **Physica E: Low-dimensional Systems and Nanostructures**, 2002. 13(2-4): p. 1212-1215.
- [28] Schallenberg, T., et al., *Shadow mask technology*. **Thin Solid Films**, 2002. 412(1-2): p. 24-29.
- [29] Burger, G.J., et al., *High-resolution shadow-mask patterning in deep holes and its application to an electrical wafer feed-through*. **Sensors and Actuators A: Physical**, 1996. 54(1-3): p. 669-673.

- [30] Brugger, J., et al., *Resistless patterning of sub-micron structures by evaporation through nanostencils*. **Microelectronic Engineering**, 2000. 53(1-4): p. 403-405.
- [31] Tixier, A., et al., *A silicon shadow mask for deposition on isolated areas*. **Journal of Micromechanics and Microengineering**, 2000. 10(2): p. 157-162.
- [32] Van den Boogaart, M.A.F., et al., *Corrugated membranes for improved pattern definition with micro/nanostencil lithography*. **Sensors and Actuators A: Physical**, 2006. 130-131: p. 568-574.
- [33] Lishchynska, M., M.A.F. van den Boogaart, and J. Brugger. *Simulation Study on Mechanical Stabilization of MEMS Stencils for Nanolithography*. in *Micromechanics Europe*. 2005. **Gothenburg, Sweden**.
- [34] Van den Boogaart, M.A.F., L.M. Doeswijk, and J. Brugger, *Silicon supported membranes for improved large-area and high-density nanostencil lithography*. **Microelectromechanical Systems, Journal of**, 2006. 15(6): p. 1663-1670.
- [35] Van den Boogaart, M.A.F., L.M. Doeswijk, and J. Brugger, *Silicon supported membranes for improved large-area and high-density nanostencil lithography*. **Microelectromechanical Systems, Journal of**, 2005. (submitted).
- [36] C.M. Lieber and Z.L. Wang, "MRS Bull. 32, 99-104 (2007). *Functional Nanowires*. **MRS Bulletin**, 2007. 32: p. 99-104.
- [37] F. Patolsky, B.P.T., G. Zheng and C.M. Lieber, *Nanowire-Based Nanoelectronic Devices in the Life Sciences*. **MRS Bulletin**, 2007. 32: p. 142-149.
- [38] Cui, Y., et al., *Doping and Electrical Transport in Silicon Nanowires*. **J. Phys. Chem. B** 2000. 104(22): p. 5213-5216.
- [39] Huang, Y., et al., *Logic Gates and Computation from Assembled Nanowire Building Blocks*. **Science**, 2001. 294(5545): p. 1313-1317.
- [40] Duan, X., et al., *Indium phosphide nanowires as building blocks for nanoscale electronic and optoelectronic devices*. **Nature**, 2001. 409(6816): p. 66-69.
- [41] Cui, Y., et al., *Nanowire Nanosensors for Highly Sensitive and Selective Detection of Biological and Chemical Species*. **Science**, 2001. 293(5533): p. 1289-1292.
- [42] Zhiyong, F. and G.L. Jia, *Gate-refreshable nanowire chemical sensors*. **Appl. Phys. Lett**, 2005. 86(12): p. 123510.
- [43] Tong, H.D. and H.V. Jansen, *Simple Technique for Direct Patterning of Nanowires using a Nanoslit Shadow Mask*, in *Transducers'07*. 2007 Lyon, France.
- [44] Speets, E.A., et al., *Formation of Metal Nano- and Micro-patterns on Self-Assembled Monolayers Using Pulsed Laser Deposition through Nanostencils and Electroless Deposition*. **Advanced Functional Materials**, 2006. 16(10): p. 1337 - 1342.
- [45] Cojocar, C.-V., et al., *Complex oxide nanostructures by pulsed laser deposition through nanostencils*. **Applied Physics Letters**, 2005. 86(18): p. 183107-3.
- [46] Jang, J., *Displays develop a new flexibility*. **Materials Today**, 2006. 9: p. 46-52.
- [47] Shaw, J.M. and P.F. Seidler, *Organic electronics: Introduction*. **IBM Journal of Research and Development**, 2001. 45(1): p. 3-9.
- [48] Tsuyoshi, S., et al., *Bending experiment on pentacene field-effect transistors on plastic films*. **Applied Physics Letters**, 2005. 86(7): p. 073511.
- [49] Racz, Z., et al., *Nanofabrication using nanotranslated stencil masks and lift off*. **Journal of Vacuum Science and Technology**, 2004. 22(1): p. 74-76.
- [50] Tsang, W.T. and A.Y. Cho, *Molecular beam epitaxial writing of patterned GaAs epilayer structures (for integrated optics)*. **Applied Physics Letters**, 1978. 32(8): p. 491-493.
- [51] Van den Boogaart, M.A.F., *Stencil Lithography: An ancient technique for advanced micro- and nanopatterning*. **Series in Microsystems**, ed. P.A. Besse, et al. Vol. 20. 2006, Konstanz: Hartung-Gorre Verlag. 181.
- [52] Van den Boogaart, M.A.F., *Stencil Lithography: An ancient technique for advanced micro- and nanopatterning*. 2006, EPFL: Lausanne. p. 181

Step and stamp imprint lithography

Tomi Haatainen, Päivi Majander and Jouni Ahopelto
 VTT, Technical Research Centre of Finland (Finland)
 Gilbert Lecarpentier
 SUSS Microtec S.A.S. (France)

Foreword

We describe two methods for nanopatterning of large areas, thermal and UV step and stamp imprint lithography (SSIL). The tool Nanoimprint Stepper (NPS300) is easily configured to both techniques. Results on CD uniformity and overlay accuracy in thermal NIL is presented.

Introduction

Conventionally, nano scale geometries have been realised using e-beam lithography, but for industrial production this method is too slow. Other microelectronics equipment and methods can be used to produce sub-100 nm line widths, but such equipment are often very expensive. Furthermore, these methods are not easily adaptable for patterning on new functional materials or using 3D geometries. During the past ten years lots of new ideas for the nanopatterning has been invented. Some of them are still in the stage of a potential to be realised, some of them already serving research and industry.

Nanoimprint lithography, based on mechanical embossing, has several different approaches, but a rough division to cold and hot embossing techniques can be made. The principle is the usage of a stamp, also called as a mould or a template, with 2D or 3D nanoscale patterns, which is pressed onto a polymer. The pattern remains in the polymer, which is then hardened (cured) either by cooling down to room temperature or by UV light. In the case of using temperature change for the moulding, the material used is a thermoplastic polymer, which becomes ductile when heated above its glass transition temperature. The other option is to use a low viscosity monomer which is polymerized and thereby cured by UV light exposure.

We present two methods based on nanoimprint lithography, the thermal and UV step and stamp imprint lithography, SSIL. In step and stamp imprint lithography, SSIL, the idea is to pattern the polymer layer using a small chip size stamp and repeat the imprint process steps sequentially so that finally the pattern is multiplied onto the whole substrate area [1-3]. Both thermoplastic and UV curable materials can be used. Since the first step and stamp imprint tests by using a flip chip bonder, the method is now developed into a stage where a dedicated commercial device Nano Imprinting Stepper (NPS300) is available for both research and industrial use [4]. Results on the CD uniformity study and pattern overlay by thermal SSIL are reported.

Thermal SSIL

The principle of step and stamp imprint lithography is presented in Fig. 1 page 29. A small silicon chip with a size of few square millimetres is used as an imprint stamp. It is

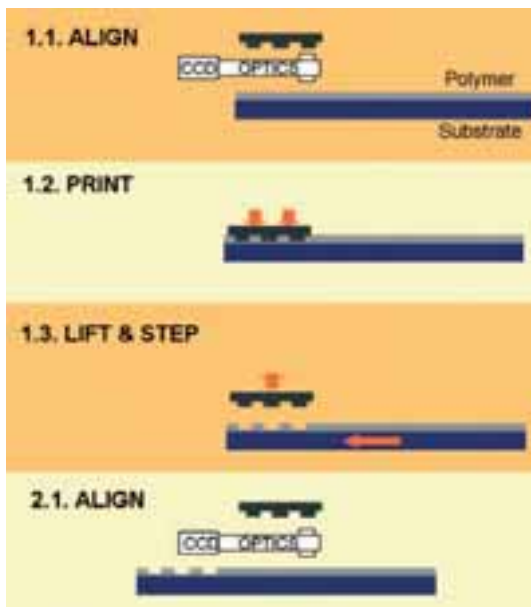


Figure 1: The principle of step and stamp imprint lithography

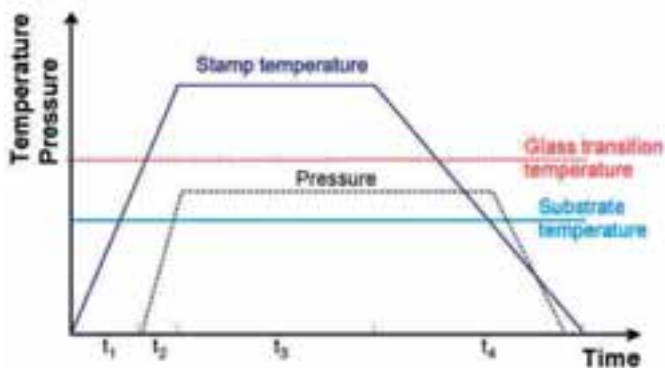


Figure 2: Temperature and force during one thermal SSIL cycle.

attached to a 50x50 mm² silicon carbide, SiC, support by adhesive or using an automatic stamp pick up system. The substrate, max. 300 mm size, is usually a silicon or glass wafer with a thermoplastic resin on top. We have used PMMA, a fluoro-resin by Asahi Glass and the mr-I 7000 and mr-I 8000 series resins (microresist technology). A temperature and pressure profile of one imprint cycle is shown in **Fig. 2**. Depending on the polymer used, the stamp is heated well above the glass transition temperature (T_g) and pressed onto the polymer at the same time. The substrate temperature is heated close to the glass transition temperature and kept constant during the imprinting. With mr-I 7000 series materials ($T_g = 60^\circ\text{C}$) the imprint temperature used is 120-140°C. The force and imprint time is optimised according to the stamp and pattern size. Finally the stamp is cooled down below the glass transition temperature and slowly detached from the polymer. The substrate is then moved to a new imprint position and the step and stamp cycle repeated. The total time of one imprint cycle is about 60 s.

Thermal SSIL provides a simple, versatile method for nanopatterning. The method is excellent for the replication of small patterns onto large area and could be used for the production of large area stamps [5]. The layout of the wafer is easily modified with a programmable tool. Possible applications are foreseen in optics, photonics, micro- and nanoelectronics.

UV SSIL

The UV SSIL is based on the idea of Step and Flash Imprint Lithography, SFIL, presented originally by J.Haisma et al. [6] The principle of UV SSIL is shown in **Fig. 3 page 30**.

For UV SSIL a transparent stamp is required, since the light source is placed behind the stamp. Normally the stamp material is either quartz or transparent polymer. As an imprint material we have used e.g. NIF-A-1 (Asahi Glass) due to its low viscosity and good anti-sticking properties. The resist is dispensed onto the substrate using a dedicated dispensing system of the imprint tool. The dispenser is programmable and can place the resist drops onto predefined sites of the substrate. The stamp is then brought to contact with the resist and the force slowly rai-

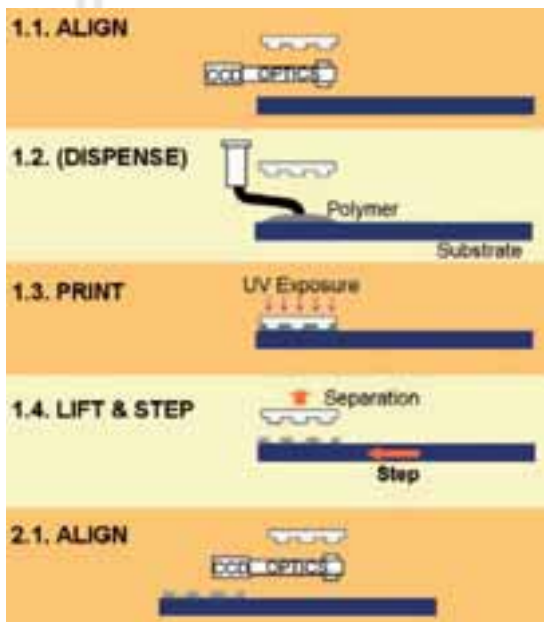


Figure 3: The principle of UV step and stamp imprint lithography.

sed as required. The sensitivity of the NIF-A-1 resist is $441\text{mJ}/\text{cm}^2$ at 365 nm and the exposure intensity on the led array is over $120\text{ mW}/\text{cm}^2$ (wavelength $375 \pm 15\text{ nm}$). The UV exposure required to cure the polymer is only few seconds. The stamp is finally detached of the polymer and ready for the next imprint cycle.

With UV SSIL there is no need for temperature change and thereby the process time compared to thermal SSIL is reduced. This enables also the use of substrates which

are sensitive to higher temperatures. The materials used have low viscosity and thereby even relatively large cavities are easily filled.

The step and stamp imprint tool, NPS300

The Nano Imprinting Stepper, NPS 300 is a tool based on the flip chip bonder and is actually capable for both imprinting and flip chip bonding. Some of the key features are listed below:

- High Alignment Accuracy
- Unmatched sub-20 nm replication capability
- Submicron Stamp-to-Wafer alignment with state-of-the-art pattern recognition system
- 250 nm overlay accuracy
- High Process Flexibility
- Various Nanoimprint processes such as thermal NIL, UV-NIL and Soft Lithography can be performed on the same platform
- Unique ability to sequentially pattern large areas to features existing on the substrate
- Imprinting force from 5 N up to 4 kN with self leveling for uniformity of the residual layer
- Possibility to add inert gas
- Fluid dispense before or after alignment
- Stamp size up to 100 mm
- Substrate up to 300 mm round or square

The advantage of NPS300 is its flexibility. The imprint arm is easily configured into UV or thermal SSIL mode. The manual loading is simple, but the machine can be equip-

Advertisement

NANOSOLUTIONS
by
ORSAY PHYSICS

**LEADER IN ION
AND ELECTRON
BEAM TECHNOLOGY**

The innovative Canion FIB range

Owing to its experience and flexibility, Orsay Physics has developed high performance and high quality ion / electron columns, that can be customised to every application.

Please contact us for more information :
Orsay Physics, Z.A. Saint Charles, Chemin des Michels, F-13710 Fuveau
Tel. +33 442 538 090 - Fax +33 442 538 091 - E-mail : nano@orsayphysics.com

ped with an automatic wafer loading system as well. Several different stamps can be used simultaneously because of the automated stamp pick up system. The programming, changing process parameters, defining the imprint sites is simple and fast, which make the tool suitable for both industrial and research use.

CD uniformity study

For the CD uniformity study a 100 mm silicon wafer was coated with a 300 nm layer of mr-I 7030 thermoplastic resin and baked on a hotplate at 140 °C for 3 min. The resist was then patterned with a stamp containing a grating of sub-200 nm lines (Fig. 4) by SSIL using NPS300. The temperature of the stamp was elevated to 140 °C before contact. The temperature was kept at 140 °C for 40 s at 3 MPa pressure and cooled down to 60 °C before releasing contact. The cycle time for one step was 80 s excluding time for chuck and imprinting arm movement. The final pattern in the substrate consisted of a matrix of 200 imprinted gratings with 5 mm pitch. A SEM image of a part of the grating is shown in Fig. 5.

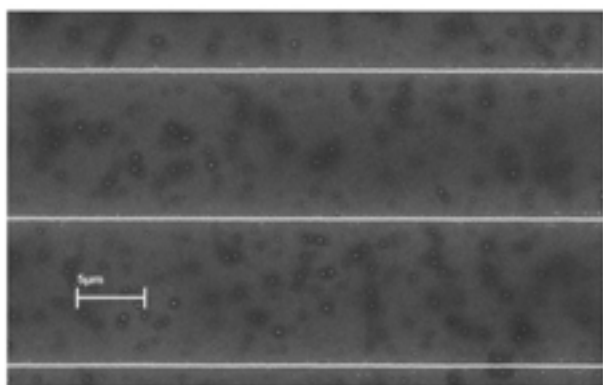


Figure 4: A SEM image of a silicon stamp with sub-200 nm wide lines of the grating.

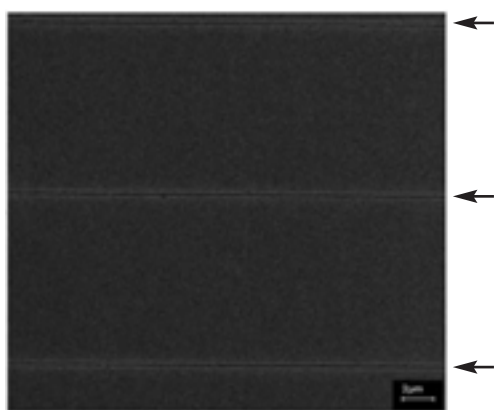


Figure 5: A SEM image of a grating etched into silicon substrate using SSIL patterned mr-I 7030 as an etch mask in CHF₃/Ar plasma.

The residual layer thickness was measured by AFM. After the residual layer removal (O₂ plasma, 3s, Plasmalab80Plus RIE) the imprinted gratings were transferred into silicon substrate by dry etching in CF₄/Ar for 3 min. The depth of the resulting trenches was 120 nm. The feature polarity of the master was turned in the substrate because of the use of an imprinted resist.

The linewidths of etched trenches were measured by

SEM (LEO1560) over the 100 mm wafer in 17 points. The distance of the adjacent measurement points is about 10 mm. The linewidth varied from 161 nm to 180 nm. The average line width is 168 nm with standard deviation of 5.2 nm.

Pattern overlay with NPS300

Overlay accuracy was tested by imprinting the second pattern layer into UV-patterned wafer with alignment marks using automatic alignment option of NPS300 Nano imPrint Stepper. Both the stamp and substrate had cross shaped alignment marks (Fig. 6). The error was estimated by measuring the shift in x and y direction between the imprinted and UV-patterned marks.

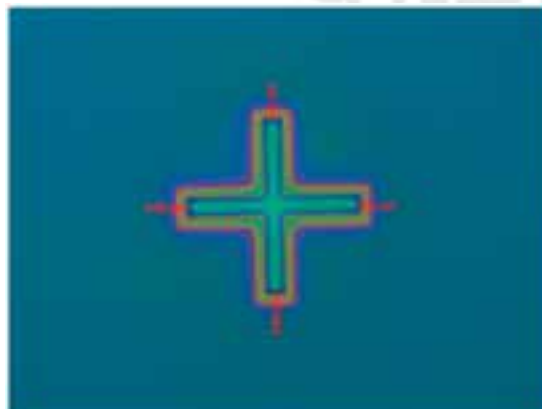


Figure 6: A micrograph of an imprinted alignment mark in the mr-I 7030 (300nm layer).

Minimum features imprinted by SSIL

The minimum features size achieved by SSIL is below 10 nm. The silicon stamp with sub-10 nm diameter pillars was patterned by electron beam lithography and dry oxidation. The oxidation step was used to shrink the features to final size below 10 nm. The features in the stamp were imprinted onto a silicon substrate coated with 300 nm thick layer of mr-I 7030 resist. In Fig. 7 a SEM image of both the stamp and imprinted pattern is presented.

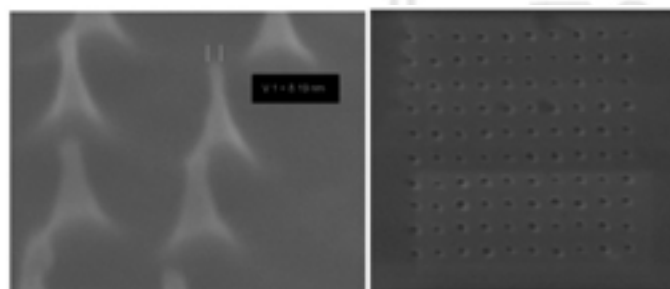


Figure 7: SEM images of sub-10 nm silicon pillars in the stamp fabricated by electron beam lithography and dry oxidation (left) and sub-10 nm holes imprinted into the mr-I 7030 resist by SSIL (right).

Field stitching with NPS300

We studied the possibility of imprinting patterns very close to each other and found out that even stitching of patterns is possible by using thermal SSIL with relatively high overlay accuracy.

For this study a 100 mm silicon wafer was coated with

A new sister journal
of the physica status
solidi journals –
solid state at its best!

Call for Papers



- **Editor-in-Chief**
Martin Stutzmann, München, GER
- **Regional Editors**
Martin S. Brandt, München, GER
Shuit-Tong Lee, Hongkong, CN
Pablo Ordejón, Barcelona, ES
Michael Shur, Troy, USA
John I. B. Wilson, Edinburgh, UK
- **Further members
of the Editorial Board**
Elvira Fortunato, Caparica, PT
John Robertson, Cambridge, UK
James S. Speck, Santa Barbara, USA
Christian Thomsen, Berlin, GER

Print ISSN 1862-6254
Online ISSN 1862-6270
2007. Volume 1, 6 issues.

www.pss-rapid.com

physica status solidi RRL – Rapid Research Letters, the fastest
peer-reviewed publication medium in solid state physics,

► offers extremely fast
publication times.
Typical are **less than 14
days** from submission to
online publication.

To ensure a high-quality standard
all published Letter articles
require positive approval by at
least two independent referees.

► communicates important findings
with a high degree of novelty and
need for express publication, as
well as other results of immediate
interest to the solid state physics
and materials science community.

► covers topics such as preparation,
structure, and simulation of
advanced materials, theoretical
and experimental investigations of
the atomistic and electronic struc-
ture, optical, magnetic, super-
conducting, ferroelectric and

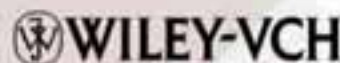
other properties of solids, nano-
structures and low-dimensional
systems as well as device
applications.

► particularly invites papers from
interdisciplinary and emerging
new areas of research.

► **Submit your
manuscript now!**

►►► Institutional customers can opt to receive
complimentary online access ◀◀◀

in 2007 and 2008. Ask your librarian to register at
www.interscience.wiley.com/newjournals



thermoplastic mr-I 7030 imprint resist and prebaked on a hot plate for 3 min at 140 °C. A silicon stamp with a grating of 1.1 mm long and 150 nm wide lines with 10µm pitch was used.

Field stitching accuracy is based on chuck stepping resolution (air bearing XY chuck and ETEL motors. Motor controllers specs: +/-20 nm positioning with 1 nm resolution). Chuck coordinate system must be adjusted to the stamp orientation in order to correct the stamp angle (Fig. 8). After stamp angle correction, automatic imprint cycles with 1080 µm steps started. The stamp temperature was raised to 130 °C. Cooling cycle of 40 s is started after 5 s contact. Pressure was released when stamp temperature of 60 °C has been reached and a new imprint cycle was thereby started.

The imprinted sample was coated with Al to improve con-

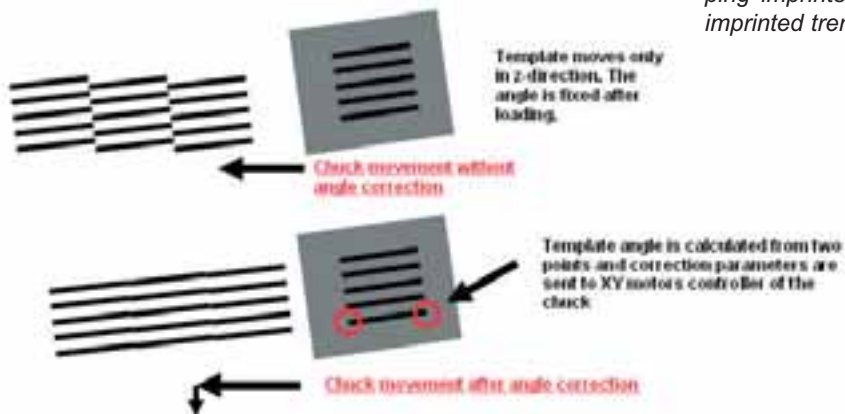


Figure 8: Procedure to correct stamp angle in stitching experiment

trast and avoid charging. Stitching error was measured by SEM measuring the error between 53 fields measured (52 overlapping points). The average error was 109 nm and standard deviation 95 nm. In Fig. 9 an optical micrograph of a part of the continuous imprinted grating is shown. When imprinting patterns side by side there is a possibi-

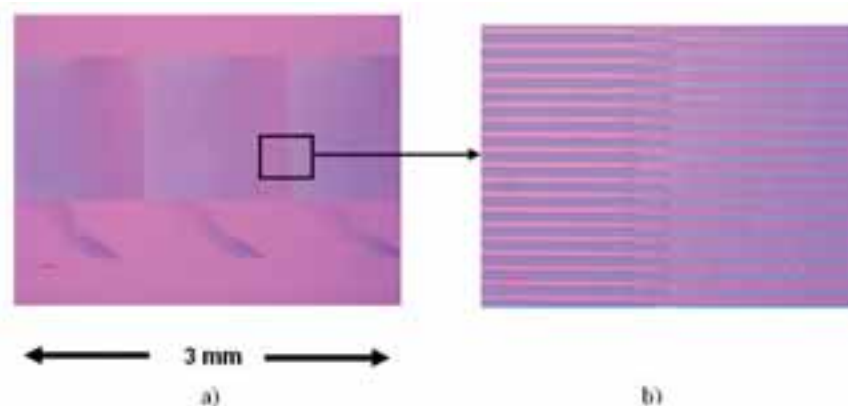


Figure 9: An optical micrograph showing a part of the continuous imprinted grating a) 20 µm overlapping area of adjacent imprints b).

ty that some resist is squeezed out below the stamp. In Fig. 10 a ridge formed to the imprinted trench due to the resist flow is shown. With a very small residual layer this effect can be even smaller.

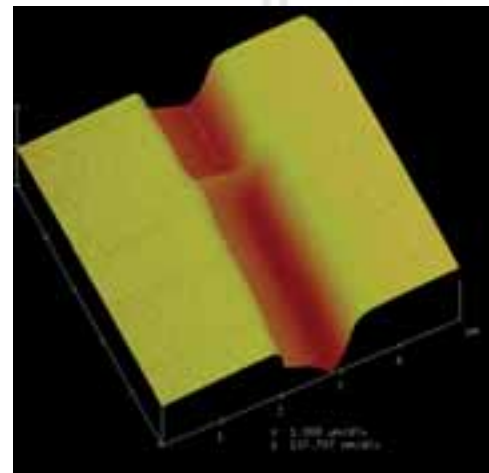


Figure 10: An AFM study of the resist flow between two overlapping imprints. A small ridge is observed in the bottom of the imprinted trench.

Conclusion

We have presented two methods based on nanoimprint lithography, thermal and UV step and stamp imprint lithography. A tool dedicated for these methods is commercially available and easily configured to both techniques. This combination provides a good basis for the development of fabrication processes for applications in optics, photonics, nano- and polymer electronics, fluidics, sensors, biotechnology, etc.

Acknowledgements

This work is done in the frame of an integrated project Emerging Nanopatterning Methods, NaPa (NMP4-CT-2003-500120), funded partially by the European Commission, which is hereby gratefully acknowledged. The content of this work is the sole responsibility of the authors.

References

- [1] Haatainen, Tomi; Ahopelto, Jouni; Gruetzner, Gabi; Fink, Marion; Pfeiffer, Karl *Emerging Lithographic Technologies IV, Proceedings of SPIE*. 3997 (2000) 874 – 880.
- [2] Haatainen, T. and Ahopelto, J., *Physica Scripta* 67 (2003) 357-360.
- [3] Ahopelto, J. and Haatainen, T., *Alternative Lithography, Unleashing the Potentials of Nanotechnology*. Kluwer Academics. New York (2003), 103 - 115
- [4] webpage: www.suss.com/products/lithography/nil/nps300
- [5] Haatainen, T., Majander, P. Mäkelä, T., Ahopelto, J. Lecarpentier, G., *Oral Presentation, The Fifth International Nanoimprint and Nanoprint Technology Conference, NNT'06, San Francisco, 15.-17.11. 2006, USA.*
- [6] M. Colburn, S. Johnson, M. Stewart, S. Damle, T. Bailey, B. Choi, M. Wedlake, T. Michaelson, S.V. Sreenivasan, J.G. Ekerdt and C.G. Willson., *Proc. SPIE* 3676(I): 379 (1999).
- [7] Haatainen, T., Majander, P., Riekkinen, T. and Ahopelto J., *Microelectron. Eng.* 83 (2006) 948-950.

Diving into the Realm of Nanosciences: Understanding of Electronic and Transport Properties of Nanotubes

Carbon nanotubes were discovered and first clearly characterized in 1991 by Professor Sumio Iijima from NEC laboratories (Japan). This discovery was made possible thanks to the use of state-of-the-art transmission electron microscopy (TEM). The spectacular impact of topology of carbon atoms on physical properties was unprecedented in Condensed Matter Physics.

This discovery has triggered during the past 10 years a tremendous amount of scientific activities first and still with a more fundamental focus, addressing nanotubes intrinsic properties, and challenging electronic properties and universal concepts of quantum transport physics by using advanced characterization techniques (transmission and tunneling microscopies, Raman studies, and mesoscopic transport measurements). In parallel, more applied research has steadily spread worldwide and carbon nanotubes are now becoming the center of concern in various electronics domains, such as interconnects, field emitters, flat displays, sensing devices, energy storage, molecular memories, and so forth.

Since more than 10 years, European researchers have actively participated to bring excellence in carbon nanotubes Science and Technology, and current activities and results are clearly amongst the leading edge contributions to deepen understanding as well as to demonstrate the possibilities for innovative carbon nanotubes-based technologies.

To date, no extensive review dealing with the established fundamentals of electronic and transport properties of carbon nanotubes, as well as their most recent advances and opened challenges was yet available for the large audience.

The recent review article by J.C. Charlier, X. Blase and S. Roche published in the issue of April-June of *Reviews of Modern Physics* is bringing a timely overview to help beginners and confirmed researchers in understanding the basic knowledge of this mainstream field of nanoscience and nanotechnology

The focus of the review is mainly theoretical, but when appropriate the relations with experimental results are mentioned. While simple band-folding arguments are invoked to rationalize how the metallic or semiconducting character of nanotubes is inferred from their topological structure, more sophisticated tight-binding and ab-initio treatments are also introduced to discuss more subtle physical effects, such as those induced by curvature, tube-tube interactions, or topological defects, whose effects become very peculiar in these low dimensional structures.

In a second part the quantum charge transport properties are overviewed. The fundamental aspects of conduction regimes and transport length scales are presented using simple models of disorder, with the derivation of a few analytic results concerning specific situations of short- and

long-range static perturbations. Further, the latest developments in semiempirical or ab-initio simulations aimed at exploring the effect of realistic static scatterers chemical impurities, adsorbed molecules, etc. or inelastic electron-phonon interactions are emphasized.

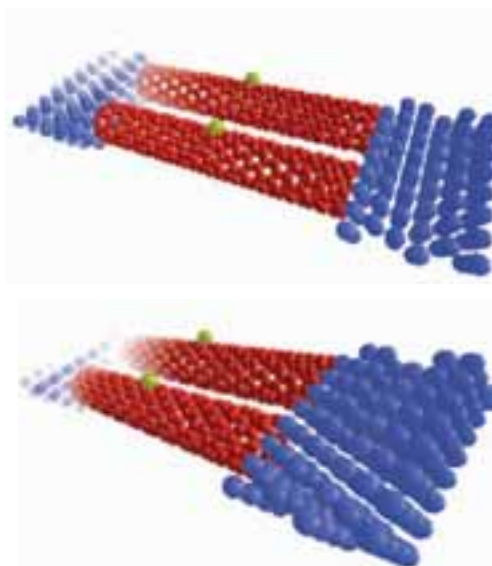
Finally, specific issues, going beyond the noninteracting electron model, are addressed, including excitonic effects in optical experiments, the Coulomb-blockade regime, and the Luttinger liquid, charge density waves, or superconducting transition.

All the people interested in carbon nanotubes and nanosciences in general are encourage to enjoy the reading of this extensive review, in which state of the art of the knowledge is given.

*REVIEWS OF MODERN PHYSICS, VOLUME 79, p677,
APRIL-JUNE 2007*

Jean-Christophe Charlier, Xavier Blase and Stephan Roche

Antonio Correia
Phantoms Foundation (Spain)



Cover Picture:

Artistic vision/representation of the nanoimprint lithography process

Design by: Enrique Sahagun (MOLE group - Universidad Autonoma de Madrid, Spain)

Special Offer

Nanotimes is happy to announce the release of a limited special edition of its famous Nt_STM simulation software based on Green: "Nt_STM_1.2"

This limited 1.2 edition is specifically designed for demanding STM experimentalists... with an exceptional **50% discount rate** on a single-station perpetual license order!

Purchase the Nt_STM_1.2 limited software package now and save up to 50% off the regular price!!! Now means from July 1st to October 31th 2007.

And if you're among the first 50 buyers, your reduction rate will climb up to 75% and you will receive an additional bonus prize (exclusive).

And there's even more for the multi-station license buyers: buy one now and get one free!

For more details about this special offer and the bonus prize and/or to purchase your software now, please contact Marianne:

- by email at sales@nanotimes.fr
- or by phone at +33 9 52 45 51 77

NB: This special offer does not include software services and maintenance.

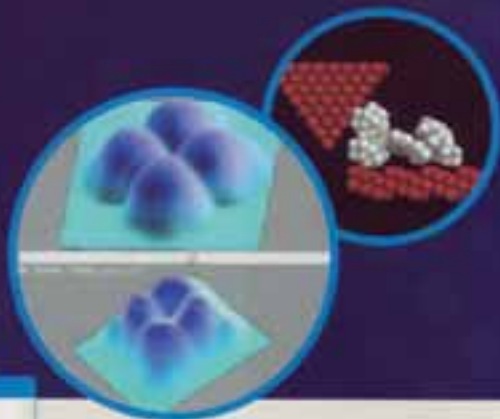


Incubateur Midi-Pyrénées
29, rue Jeanne Marvig
31400 Toulouse

Tel: +33 1038 72 45 51 77
Fax: +33 1035 34 31 68 16
info@nanotimes-corp.com

www.nanotimes-corp.com

» SOFTWARE SOLUTIONS FOR NANOSCALE SIMULATION AND INTERPRETATION



NANO
t i m e s

Nanotimes-STM

simulates all stages of an experiment carried out with a tunnelling effect microscope (STM).

Nanotimes-STM can calculate the electrical current through any nanometrical system, by calculating the transmission of electrons between the microscope tip and the surface, and is capable of entirely reproducing the activity of an STM.

A comprehensive simulation tool,

Nanotimes-STM:

- ▶ handles all types of systems; surfaces, adsorbed molecules, atom deposits
- ▶ accurately simulates microscope experiments
- ▶ offers simple system initialisation of variables (height, current, surface) and tip course
- ▶ features step-by-step monitoring of tip course and resulting measurements
- ▶ combines easily with more complex theoretical chemistry programs for more rigorous simulations
- ▶ can be used to model, predict or validate any type of transmission experiment.

SURFACE ANALYSIS



AFM / STM

Materials, polymers, biology, electrochemistry...



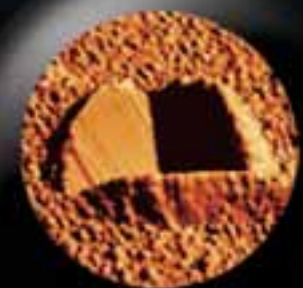
SNOM Microscopy

*Reflection, transmission, Apertureless...
SECM, Deep Trench, nanopipette probes...*



3D Optical Profilometry

*New confocal technology...
Interferometry (PSI/VSI)...*



And also...

Mechanical profilometry, nano-indentation...



ScienTec FRANCE
17 Av. des Andes - Batiment le Cèdre
91940 LES ULIS
Tel : + 33 (0)1 64 53 27 00

ScienTec IBERICA
C/Buenavista 4, Bajos
28250 Madrid - ESPAÑA
Tel : + 34 918 429 467

www.scientec.fr

info@scientec.fr